

Phase-Oscillator Computations as Neural Models of Stimulus-Response Conditioning and Response Selection[☆]

P. Suppes^a, J. Acacio de Barros^b, G. Oas^a

^a*CSLI, Ventura Hall, 220 Panama Street, Stanford University, Stanford, CA 94305-4101*

^b*Liberal Studies Program, San Francisco State University, 1600 Holloway Ave., San Francisco, CA 94132*

Abstract

The activity of collections of synchronizing neurons can be represented by weakly coupled nonlinear phase oscillators satisfying Kuramoto's equations. In this article, we build such neural-oscillator models, partly based on neurophysiological evidence, to represent approximately the learning behavior predicted and confirmed in three experiments by well-known stochastic learning models of behavioral stimulus-response theory. We use three Kuramoto oscillators to model a continuum of responses, and we provide detailed numerical simulations and analysis of the three-oscillator Kuramoto problem, including an analysis of the stability points for different coupling conditions. We show that the oscillator simulation data are well-matched to the behavioral data of the three experiments.

Keywords: learning; neural oscillators; three-oscillator Kuramoto model; stability points of the Kuramoto model; stimulus-response theory; phase representation; continuum of responses

1. Introduction

With the advent of modern experimental and computational techniques, substantial progress has been made in understanding the brain's mechanisms for learning. For example, extensive computational packages based on detailed experimental data on ion-channel dynamics make it now possible to simulate the behavior of networks of neurons starting from the flow of ions through neurons' membranes (Bower and Beeman, 2003). Yet, there is much to be determined at a system level about brain processes. This can be contrasted to the large literature in psychology on learning, psychophysics, and perception. Among the most developed behavioral mathematical models of learning are those of stimulus-response (SR) theory (Estes, 1950, 1959; Suppes, 1959, 1960; Suppes and Atkinson, 1960; Suppes and Ginsberg, 1963). (From the large SR literature, we reference here only the results we use in some detail.) In this article, we propose weakly coupled phase oscillators as neural models to do the brain computations needed for stimulus-response conditioning and response conditioning. We then use such oscillators to analyze two experiments on noncontingent probabilistic reinforcement, the first with a continuum of responses and a second with just two. A third experiment is on paired-associate learning.

The oscillator assumptions we make are broadly based on neurophysiological evidence that neural oscillators, made up of collections of synchronized neurons, are apparently ubiquitous in the brain. Their oscillations are macroscopically observable in electroencephalograms (Freeman, 1979; Gerstner and Kistler, 2002; Wright and Liley, 1995). Detailed theoretical analyses have shown that weakly interacting neurons close to a bifurcation exhibit such oscillations (Gerstner and Kistler, 2002; Hoppensteadt and Izhikevich, 1996a,b; Izhikevich, 2007). Moreover, many experiments not only provide

Email addresses: psuppes@stanford.edu (P. Suppes), barros@sfsu.edu (J. Acacio de Barros), oas@stanford.edu (G. Oas)

evidence of the presence of oscillators in the brain (Eckhorn et al., 1988; Friedrich et al., 2004; Kazantsev et al., 2004; Lutz et al., 2002; Murthy and Fetz, 1992; Rees et al., 2002; Rodriguez et al., 1999; Sompolinsky et al., 1990; Steinmetz et al., 2000; Tallon-Baudry et al., 2001; Wang, 1995), but also show that their synchronization is related to perceptual processing (Friedrich et al., 2004; Kazantsev et al., 2004; Leznik et al., 2002; Murthy and Fetz, 1992; Sompolinsky et al., 1990). They may play a role in solving the binding problem (Eckhorn et al., 1988). More generally, neural oscillators have already been used to model a wide range of brain functions, such as pyramidal cells (Lytton and Sejnowski, 1991), effects of electric fields in epilepsy (Park et al., 2003), activities in the cat visual cortex (Sompolinsky et al., 1990), learning of songs by birds (Trevisan et al., 2005), learning (Vassilieva et al., 2011), and coordinated finger tapping (Yamanishi et al., 1980). Suppes and Han (2000) showed that a small number of frequencies can be used to recognize a verbal stimulus from EEG data, consistent with the brain representation of language being neural oscillators. From a very different perspective, in Billock and Tsou (2005) synchronizing neural oscillators were used to rescale sensory information, and Billock and Tsou (2011) used synchronizing coupled neural oscillators to model Steven’s law, thus suggesting that neural synchronization is relevant to cognitive processing in the brain.

Our working hypothesis is that main cognitive computations needed by the brain for the SR experiments we consider can be modeled by weakly coupled phase oscillators that together satisfy Kuramoto’s nonlinear equations (Acebron et al., 2005; Hoppensteadt and Izhikevich, 1996a,b; Kuramoto, 1984; Strogatz, 2000; Winfree, 2002). When a stimulus is sampled, its corresponding neural oscillator usually phase locks to the response-computation oscillators. When a reinforcement occurs, the coupling strengths will often change, driven by the reinforcement oscillator. Thus, SR conditioning is represented by phase locking, driven by pairwise oscillator couplings, whose changes reflect learning.

Despite the large number of models of processing in the brain, we know of no detailed systematic efforts to fit neural oscillator models to behavioral learning data. We choose to begin with SR theory for several reasons. This theory has a solid mathematical foundation (Suppes, 2002); it has been used to predict many non trivial quantitative features of learning, especially in the form of experimentally observed conditional probabilities (Bower, 1961; Suppes and Atkinson, 1960; Suppes and Ginsberg, 1963; Suppes et al., 1964). It can also be used to represent computational structures, such as finite automata (Suppes, 1969, 2002). Furthermore, because neural oscillators can interfere (see, for example, our treatment of a continuum of responses below), they may provide a basis for quantum-like behavior in the brain (de Barros and Suppes, 2009; Suppes and de Barros, 2007), an area of considerable research in recent years (Bruza et al., 2009).

In Section 2 we start with a brief review of SR theory, followed by a detailed stochastic process version of an SR model for a continuum of responses. In Section 4 we present in some detail the neural oscillator computation for the SR continuum model. Extension to other SR models and experiments follows, as already remarked. In Section 5 we compare the computations of the oscillator simulations to empirical data from three behavioral experiments designed to test the predictions of stimulus-response theory.

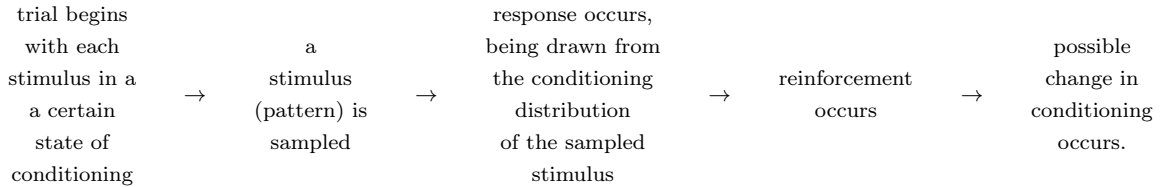
2. Stimulus-Response Theory

The first aim of the present investigation is to use the extension of stimulus-response theory to situations involving a continuum of possible responses, because the continuum case most closely corresponds to the physically natural continuous nature of oscillators. The SR theory for a finite number of responses stems from the basic paper by (Estes, 1950); the present formulation resembles most closely that given for the finite case in Suppes and Atkinson (1960, Chapter 1), and in the continuum case (Suppes, 1960).

The general experimental situation consists of a sequence of trials. On each trial the participant (in the experiment) makes a response from a continuum or finite set of possible responses; his response is followed by a reinforcing event indicating the correct response for that trial. In situations of simple learning, which are characterized by a constant stimulating situation, responses and reinforcements constitute the only observable data, but stimulus-response theory postulates a considerably more

complicated process which involves the conditioning and sampling of stimuli, which are best interpreted as patterns of stimuli, with a single pattern being sampled on each trial. In the finite case the usual assumption is that on any trial each stimulus is conditioned to exactly one response. Such a highly discontinuous assumption seems inappropriate for a continuum or a large finite set of responses, and it is replaced with the general postulate that the conditioning of each stimulus is *smear*ed over a set of responses, possibly the whole continuum. In these terms, the conditioning of any stimulus may be represented uniquely by a *smearing probability distribution*, which we also call the *conditioning distribution* of the stimulus.

The theoretically assumed sequence of events on any trial may then be described as follows:



The sequence of events just described is, in broad terms, postulated to be the same for finite and infinite sets of possible responses. Differences of detail will become clear. The main point of the axioms is to formulate verbally the general theory. As has already been more or less indicated, three kinds of axioms are needed: conditioning, sampling, and response axioms. After this development, more technically formulated probabilistic models for the different kind of experiments are given.

2.1. General Axioms

The axioms are formulated verbally but with some effort to convey a sense of formal precision.

Conditioning Axioms.

C1. For each stimulus s there is on every trial a unique conditioning distribution, called the smearing distribution, which is a probability distribution on the set of possible responses.

C2. If a stimulus is sampled on a trial, the mode of its smearing distribution becomes, with probability θ , the point (if any) which is reinforced on that trial; with probability $1-\theta$ the mode remains unchanged.

C3. If no reinforcement occurs on a trial, there is no change in the smearing distribution of the sampled stimulus.

C4. Stimuli which are not sampled on a given trial do not change their smearing distributions on that trial.

C5. The probability θ that the mode of the smearing distribution of a sampled stimulus will become the point of the reinforced response is independent of the trial number and the preceding pattern of occurrence of events.

Sampling Axioms.

S1. Exactly one stimulus is sampled on each trial.

S2. Given the set of stimuli available for sampling on a given trial, the probability of sampling a given element is independent of the trial number and the preceding pattern of occurrence of events.

Response Axioms.

R1. The probability of the response on a trial is solely determined by the smearing distribution of the sampled stimulus.

These axioms are meant to make explicit the conceptual framework of the sequence of events postulated to occur on each trial, as already described.

2.2. Stochastic Model for a Continuum of Responses

Four random variables characterize the stochastic model of the continuum-of-responses experiment: Ω is the probability space, P is its probability measure, S is the set of stimuli (really patterns of stimuli), R is the set of possible responses, E is the set of reinforcements, and \mathbf{S} , \mathbf{X} , and \mathbf{Y} , are the corresponding random variables, printed in boldface. The other random variable is the conditioning random variable \mathbf{Z} , which carries the essential information in a single parameter z_n . It is assumed that on each trial the conditioning of a stimulus s in S is a probability distribution $K_s(r|z)$, which is a distribution on possible responses x in R . So, in the experiments analyzed here, the set of responses R is just the set of real numbers in the periodic interval $[0, 2\pi]$. It is assumed that this distribution $K_s(r|z)$ has a constant variance on all trials and is defined by its mode z and variance. The mode changes from trial to trial, following the pattern of reinforcements. This qualitative formulation is made precise in what follows. The essential point is this. Since only the mode is changing, we can represent the conditioning on each trial by the random variable \mathbf{Z} . So $\mathbf{Z}_{s,n} = z_{s,n}$ says what the mode of the conditioning distribution $K_s(r|z_n)$ for stimulus s is on trial n . We subscript the notation z_n with s as well, i.e., $z_{s,n}$ when needed. Formally, on each trial n , z_n is the vector of modes (z_1, \dots, z_m) for the m stimuli in S . So $\Omega = (\Omega, P, S, R, E)$ is the basic structure of the model.

Although experimental data will be described later in this paper, it will perhaps help to give a schematic account of the apparatus which has been used to test the SR theory extensively in the case of a continuum of responses. A participant is seated facing a large circular vertical disc. He is told that his task on each trial is to predict by means of a pointer where a spot of light will appear on the rim of the disc. The participant's pointer predictions are his responses in the sense of the theory. At the end of each trial the "correct" position of the spot is shown to the participant, which is the reinforcing event for that trial.

The most important variable controlled by the experimenter is the choice of a particular reinforcement probability distribution. Here this is the noncontingent reinforcement distribution $F(y)$, with density $f(y)$, on the set R of possible responses, and "noncontingent" means that the distribution of reinforcements is not contingent on the actual responses of the participant.

There are four basic assumptions defining the SR stochastic model of this experiment.

A1. If the set S of stimuli has m elements, then $P(\mathbf{S}_n = s | s \in S) = \frac{1}{m}$.

A2. If $a_2 - a_1 \leq 2\pi$ then $P(a_1 \leq \mathbf{X}_n \leq a_2 | \mathbf{S}_n = s, \mathbf{Z}_{s,n} = z) = \int_{a_1}^{a_2} k_s(x|y) dx$.

A3. (i) $P(\mathbf{Z}_{s,n+1} = y | \mathbf{S}_n = s, \mathbf{Y}_n = y \& \mathbf{Z}_{s,n} = z_{s,n}) = \theta$

and

(ii) $P(\mathbf{Z}_{s,n+1} = z_{s,n} | \mathbf{S}_n = s, \mathbf{Y}_n = y \& \mathbf{Z}_{s,n} = z_{s,n}) = (1 - \theta)$.

A4. The temporal sequence in a trial is:

$$\mathbf{Z}_n \rightarrow \mathbf{S}_n \rightarrow \mathbf{X}_n \rightarrow \mathbf{Y}_n \rightarrow \mathbf{Z}_{n+1}. \quad (1)$$

Assumption A1 defines the sampling distribution, which is left open in Axioms S1 and S2. Assumptions A2 and A3 complement Axioms C1 and C2. The remaining conditioning axioms, C3, C4,

and C5, have the general form given earlier. The same is true of the two sampling axioms. The two axioms C5 and S2 are just *independence-of-path* assumptions. These axioms are crucial in proving that for simple reinforcement schedules the sequence of random variables which take as values the modes of the smearing distributions of the sampled stimuli constitutes a continuous-state discrete-trial Markov process.

For example, using J_n for the joint distribution of any finite sequence of these random variables and j_n for the corresponding density,

$$P(a_1 \leq \mathbf{X}_n \leq a_2 | \mathbf{S}_n = s, \mathbf{Z}_{s,n} = z) = \int_{a_1}^{a_2} j_n(x|s, z) dx = K_s(a_2; z) - K_s(a_1; z).$$

The following obvious relations for the response density r_n of the distribution R_n will also be helpful later. First, we have that

$$r_n(x) = j_n(x),$$

i.e., r_n is just the marginal density obtained from the joint distribution j_n . Second, we have “expansions” like

$$r_n(x) = \int_0^{2\pi} j_n(x, z_{s,n}) dz_{s,n},$$

and

$$r_n(x) = \int_0^{2\pi} \int_0^{2\pi} \int_0^{2\pi} j_n(x, z_{s,n}, y_{n-1}x_{n-1}) dz_{s,n} dy_{n-1} dx_{n-1}.$$

2.3. Noncontingent Reinforcement

Noncontingent reinforcement schedules are those for which the distribution is independent of n , the responses, and the past. We first use the response density recursion for some simple, useful results which do not explicitly involve the smearing distribution of the single stimulus. There is, however, one necessary preliminary concerning derivation of the asymptotic response distribution in the stimulus-response theory.

Theorem 1. *In the noncontingent case, if the set of stimuli has m elements,*

$$r(x) = \lim_{n \rightarrow \infty} r_n(x) = \frac{1}{m} \sum_{s \in S} \int_0^{2\pi} k_s(x; y) f(y) dy. \quad (2)$$

We now use (2) to establish the following recursions. In the statement of the theorem $E(\mathbf{X}_n)$ is the expectation of the response random variable \mathbf{X}_n , $\mu_r(\mathbf{X}_n)$ is its r -th raw moment, $\sigma^2(\mathbf{X}_n)$ is its variance, and \mathbf{X} is the random variable with response density r .

Theorem 2.

$$r_{n+1}(x) = (1 - \theta)r_n(x) + \theta r(x), \quad (3)$$

$$E(\mathbf{X}_{n+1}) = (1 - \theta)E(\mathbf{X}_n) + \theta E(\mathbf{X}), \quad (4)$$

$$\mu_r(\mathbf{X}_{n+1}) = (1 - \theta)\mu_r(\mathbf{X}_n) + \theta\mu_r(\mathbf{X}), \quad (5)$$

$$\sigma^2(\mathbf{X}_{n+1}) = (1 - \theta)\sigma^2(\mathbf{X}_n) + \theta\sigma^2(\mathbf{X}) + \theta(1 - \theta)[E(\mathbf{X}_n) - E(\mathbf{X})]^2 \quad (6)$$

Because (3)-(5) are first-order difference equations with constant coefficients we have as an immediate consequence of the theorem:

Corollary 1.

$$r_n(x) = r(x) - [r(x) - r_1(x)](1 - \theta)^{n-1}, \quad (7)$$

$$E(\mathbf{X}_n) = E(\mathbf{X}) - [E(\mathbf{X}) - E(\mathbf{X}_1)](1 - \theta)^{n-1}, \quad (8)$$

$$\mu_r(\mathbf{X}_n) = \mu_r(\mathbf{X}) - [\mu_r(\mathbf{X}) - \mu_r(\mathbf{X}_1)](1 - \theta)^{n-1} \quad (9)$$

Although the one-stimulus model and the N -stimulus model both yield (3)–(9), predictions of the two models are already different for one of the simplest sequential statistics, namely, the probability of two successive responses in the same or different subintervals. We have the following two theorems for the one-stimulus model. The result generalizes directly to any finite number of subintervals.

Theorem 3. *For noncontingent reinforcement*

$$\begin{aligned} & \lim_{n \rightarrow \infty} P(0 \leq \mathbf{X}_{n+1} \leq c, 0 \leq \mathbf{X}_n \leq c) \\ &= \theta R(c)^2 + (1 - \theta) \frac{1}{m^2} \sum_{s' \in S} \sum_{s \in S} \int_0^c \int_0^c \int_0^{2\pi} k_s(x; z) k_{s'}(x'; z) f(z) dx dx' dz, \end{aligned} \quad (10)$$

and

$$\begin{aligned} & \lim_{n \rightarrow \infty} P(0 \leq \mathbf{X}_{n+1} \leq c, c \leq \mathbf{X}_n \leq 2\pi) \\ &= \theta R(c)[1 - R(c)] + (1 - \theta) \frac{1}{m^2} \sum_{s' \in S} \sum_{s \in S} \int_0^c \int_c^{2\pi} \int_0^{2\pi} k_s(x; z) k_{s'}(x'; z) f(z) dx dx' dz, \end{aligned} \quad (11)$$

where

$$R(c) = \lim_{n \rightarrow \infty} R_n(c).$$

We conclude the treatment of noncontingent reinforcement with two expressions dealing with important sequential properties. The first gives the probability of a response in the interval $[a_1, a_2]$ given that on the previous trial the reinforcing event occurred in the interval $[b_1, b_2]$.

Theorem 4.

$$\begin{aligned} & P(a_1 \leq \mathbf{X}_{n+1} \leq a_2 | b_1 \leq Y_n \leq b_2, a_3 \leq \mathbf{X}_n \leq a_4) \\ &= (1 - \theta)[R_n(a_2) - R_n(a_1)] + \frac{\theta}{F(b_2) - F(b_1)} \frac{1}{m} \sum_{s \in S} \int_{a_1}^{a_2} \int_{b_1}^{b_2} k_s(x; y) f(y) dx dy. \end{aligned} \quad (12)$$

The expression to which we now turn gives the probability of a response in the interval $[a_1, a_2]$ given that on the previous trial the reinforcing event occurred in the interval $[b_1, b_2]$ and the response in the interval $[a_3, a_4]$.

Theorem 5.

$$\begin{aligned} & P(a_1 \leq \mathbf{X}_{n+1} \leq a_2 | b_1 \leq Y_n \leq b_2, a_3 \leq \mathbf{X}_n \leq a_4) \\ &= \frac{(1 - \theta)}{R_n(a_4) - R_n(a_3)} \frac{1}{m^2} \sum_{s' \in S} \sum_{s \in S} \int_0^{2\pi} \int_{a_1}^{a_2} \int_{a_3}^{a_4} \int_a^b k_s(x; z) k_{s'}(x'; z) g_n(z) dx dx' dz. \\ & \quad + \frac{\theta}{F(b_2) - F(b_1)} \frac{1}{m} \sum_{s \in S} \int_{a_1}^{a_2} \int_{b_1}^{b_2} k_s(x; z) f(y) dx dy. \end{aligned} \quad (13)$$

2.4. More General Comments on SR theory

The first general comment concerns the sequence of events occurring on each trial, represented earlier by equation (1) in Assumption A4 of the stochastic model. We want to examine in a preliminary way when brain computations, and therefore neural oscillators, are required in this temporal sequence.

- (i) \mathbf{Z}_n sums up previous conditioning and does not represent a computation on trial n ;
- (ii) \mathbf{S}_n , which represents the experimentally unobserved sampling of stimuli, really patterns of stimuli, uses an assumption about the number of stimuli, or patterns of them, being sampled in an experiment; the uniform distribution assumed for this sampling is artificially simple, but computationally useful; in any case, no brain computations are modeled by oscillators here, even though a complete theory would be required;
- (iii) \mathbf{X}_n represents the first brain computation in the temporal sequence on a trial for the stochastic model; this computation selects the actual response on the trial from the conditioning distribution $k_s(x|z_{s,n})$, where s is the sampled stimulus on this trial ($\mathbf{S}_n = s$); this is one of the two key oscillator computations developed in the next section;
- (iv) \mathbf{Y}_n is the reinforcement random variable whose distribution is part of the experimental design; individual reinforcements are external events totally controlled by the experimenter, and as such require no brain computation by the participant;
- (v) \mathbf{Z}_{n+1} summarizes the assumed brain computations that often change at the end of a trial the state of conditioning of the stimulus s sampled on trial n ; in our stochastic model, this change in conditioning is represented by a change in the mode $z_{s,n}$ of the distribution $K_s(x|z_{s,n})$. From the assumptions A1-4 and the general independence-of-path axioms, we can prove that the sequence of random variable Z_1, \dots, Z_n, \dots is a first-order Markov process (Suppes, 1960).

The second general topic is of a different sort. It concerns the important concept of *activation*, which is a crucial but implicit aspect of SR theory. Intuitively, when a stimulus is sampled, an image of that stimulus is activated in the brain, and when a stimulus is not sampled on a trial, its conditioning does not change, which implies a constant state of low or no activity for the brain image of that unsampled stimulus.

Why is this concept of activation important for the oscillator or other physical representations of how SR theory is realized in the brain? Perhaps the most fundamental reason arises from our general conception of neural networks, or, to put it more generally, “purposive” networks. For large networks, i.e., ones with many nodes, it is almost always unrealistic to have all nodes active all of the time. For biological systems such an inactive state with low consumption of energy is necessary in many situations. The brain certainly seems to be a salient example. Without this operational distinction, imagine a human brain in which episodic memories of many past years were as salient and active as incoming perception images. This critical distinction in large-scale networks between active and inactive nodes is often ignored in the large literature on artificial neural networks, but its biological necessity has long been recognized, and theoretically emphasized in psychology since the 1920s. In this paper, we accept the importance of activation, but do not attempt an oscillator representation of the physical mechanism of activating brain images arising from perceived stimuli. This also applies to the closely related concept of *spreading* activation, which refers to brain images perceptually activated associatively by other brain images, which are not themselves directly activated by perception.

3. Model overview

The neural oscillator model we developed is significantly more complex, both mathematically and conceptually, than SR theory. Furthermore, it requires the use of some physical concepts that are probably unfamiliar to some readers of this journal. So, before we present the mathematical details of the model in Section 4, we introduce here the main ideas behind the oscillator model in a conceptual

way, and show each step of the computation and how it relates to SR theory. Schematically, the oscillator model corresponds to the following steps, described in more detail later in this section.

1. Trial n starts with a series of stimulus and response neural oscillators connected through excitatory and inhibitory couplings.
2. A stimulus oscillator is activated, and by spreading activation the response oscillators.
3. Activation leads to new initial conditions for the stimulus and response oscillators; we assume such conditions are normally distributed.
4. The stimulus and response neural oscillators evolve according to non-linear deterministic differential equations.
5. After a response time Δt_r , relative phase relations between the stimulus and response oscillators determine the response made on trial n .
6. The reinforcement oscillator is then activated at time t_e after the response has occurred.
7. Activation of the reinforcement oscillator leads to other new “initial” conditions at t_e ; such conditions we again assume are normally distributed.
8. The stimulus, response, and reinforcement neural oscillators, as well as their couplings, evolve according to nonlinear deterministic differential equations.
9. After a time interval Δt_e , reinforcement is completed, and the excitatory and inhibitory couplings may have changed.

Step 1 corresponds to the random variable \mathbf{Z}_n in equation (1), Step 2 to \mathbf{S}_n , Steps 3–5 to \mathbf{X}_n , and Steps 6–9 to \mathbf{Y}_n and \mathbf{Z}_{n+1} . Let us now look at each process in more detail, from a neural point of view.

Sampling. We start the description of our model by the sampling of a stimulus, \mathbf{S}_n . For each element s of the set of stimuli S , we assume the existence of a corresponding neural phase oscillator, φ_s . The sampling of a specific s thus activates the neural oscillator φ_s . As mentioned before, we do not present a detailed theory of activation or spreading activation, but simply assume that for each trial a φ_s is activated according to a uniform distribution, consistent with \mathbf{S}_n . Once an oscillator φ_s is activated, this activation spreads to those oscillators coupled to it, including the response oscillators φ_{r_1} and φ_{r_2} .

Response. In our model, we simplify the dynamics by considering only two response oscillators, φ_{r_1} and φ_{r_2} . We should emphasize that, even though we are talking about two response oscillators, we are not thinking of them as modeling two responses, but a continuum of responses. Intuitively, we think of φ_{r_1} as corresponding to a certain extreme value in a range of responses, for example 1, and φ_{r_2} to another value, say -1 .¹

Couplings between the stimulus and response oscillators can be of two types: excitatory or inhibitory. Excitatory couplings have the effect of promoting the synchronization of two oscillators in a way that brings their phases together. Inhibitory couplings also promote synchronization, but in such a way that the relative phases are off by π . If oscillators are not at all coupled, then their dynamical evolution is dictated by their natural frequencies, and no synchronization appears. Figure 1 shows the evolution for three uncoupled oscillators. However, if a system starts with oscillators randomly close to each other in phase, when oscillators are coupled, some may evolve to be in-phase or out-of-phase.

To describe how a response is computed, we first discuss the interference of neural oscillators. At the brain region associated to φ_{r_1} , we have the oscillatory activities due not only to φ_{r_1} but also to φ_s , since the stimulus oscillator is coupled to φ_{r_1} . This sum of oscillations may result in either constructive or destructive interference. Constructive interference will lead to stronger oscillations at φ_{r_1} , whereas destructive interference will lead to weaker oscillations. So, let us assume that the couplings between φ_s and the response oscillators are such that the stimulus oscillator synchronizes in-phase with φ_{r_1}

¹In reality, responses in our model have the same topological structure as the unit circle. See Section 4 for details.

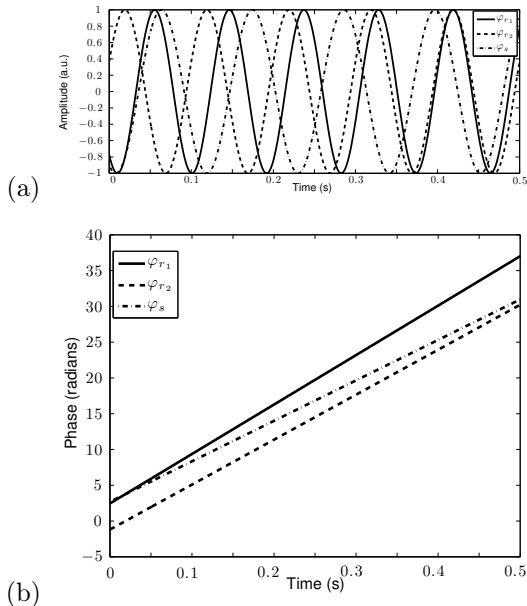


Figure 1: Time evolution of three oscillators represented by $A(t) = \cos(\varphi(t))$, where $\varphi(t)$ is the phase. Graph (a) shows the oscillations for uncoupled oscillators with frequencies 11 Hz (solid line), 10 Hz (dashed), and 9 Hz (dash-dotted). Notice that though the oscillators start roughly in phase, they slowly dephase as time progresses. Graph (b) shows the phases $\varphi(t)$ of the same three oscillators in (a).

and out-of-phase with φ_{r_2} . Synchronized in-phase oscillators correspond to higher intensity than out-of-phase oscillators. The dynamics of the system is such that its evolution leads to a high intensity for the superposition of the stimulus φ_s and response oscillator φ_{r_1} (constructive interference), and a low intensity for the superposition of φ_s and φ_{r_2} (destructive interference). Thus, in such a case, we say that the response will be closer to the one associated to φ_{r_1} , i.e., 1. Figure 2 shows the evolution of coupled oscillators, with couplings that lead to the selection of response 1.

From the previous paragraph, it is clear how to obtain answers at the extremes values of a scale (-1 and 1 in our example). However, the question remains on how to model a continuum of responses. To examine this, let us call I_1 the intensity at φ_{r_1} due to its superposition with φ_s , and let us call I_2 the intensity for φ_{r_2} and φ_s . Response 1 is computed from the oscillator model when I_1 is maximum and I_2 is minimum, and -1 vice versa. But those are not the only possibilities, as the phase relations between φ_s and the response oscillators do not need to be such that when I_1 is maximum I_2 is minimum. For example, it is possible to have $I_1 = I_2$. Since we are parametrizing 1 (-1) to correspond to a maximum for I_1 (I_2) and a minimum for I_2 (I_1), it stands to reason that $I_1 = I_2$ corresponds to 0 . More generally, by considering the relative intensity between I_1 and I_2 , defined by

$$b = \frac{I_1 - I_2}{I_1 + I_2}, \quad (14)$$

which can be rewritten as

$$b = \frac{I_1/I_2 - 1}{I_1/I_2 + 1} \text{ if } I_2 \neq 0,$$

any value between -1 and 1 may be computed by the oscillator model. For example, when $I_2 = (1/3)I_1$, we see from equation (14) that the computed response would be $1/2$, whereas $I_2 = 3I_1$ would yield $-1/2$. We emphasize, though, that there is nothing special about -1 and 1 , as those were values that we selected to parametrize the response; we could have selected α and β as the range for our continuum of responses by simply redefining b in Eq. (14).

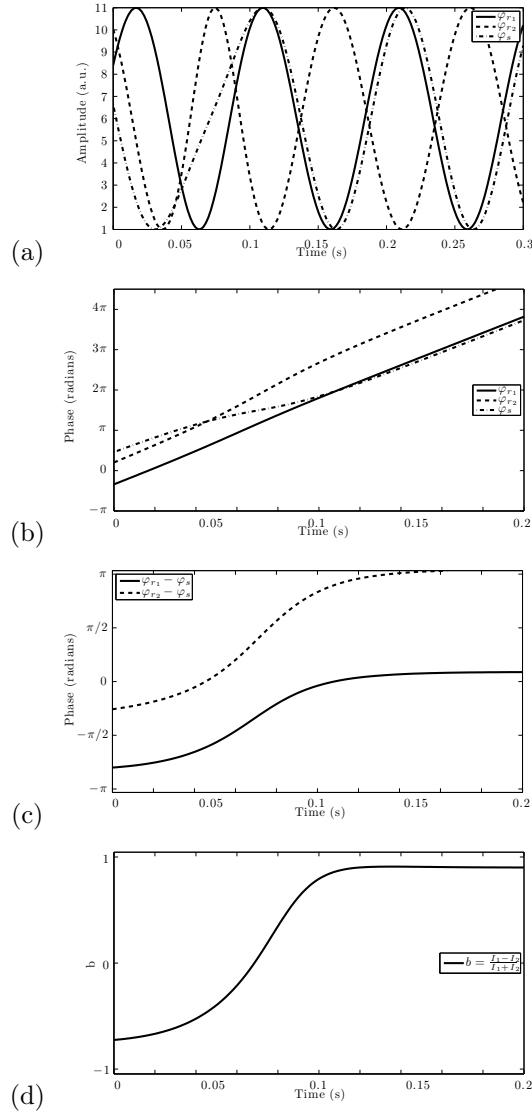


Figure 2: Same three oscillators as in Figure 1, but now coupled. We see from (a) that even though the system starts with no synchrony, as oscillators have different phases and natural frequencies, very quickly (after 100 ms) the stimulus oscillator s (dash-dotted line) becomes in synch and in phase with response r_1 (solid line), while at the same time becoming in synch but off phase with r_2 . This is also represented in (b) by having one of the oscillators approach the trajectory of the other. Graph (c) shows the phase differences between the stimulus oscillators s and r_1 (solid line) and s and r_2 (dashed line). Finally, (d) shows the relative intensity of the superposition of oscillators, with 1 corresponding to maximum intensity at r_1 and minimum at r_2 and -1 corresponding to a maximum in r_2 and minimum in r_1 . As we can see, the couplings lead to a response that converges to a value close to 1.

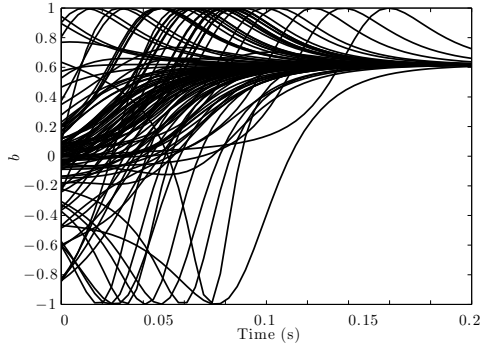


Figure 3: Response computation trajectories for 100 randomly-selected initial conditions for an oscillator set conditioned to the response 1/2.

It can now be seen where the stochastic characteristics of the model appear. First, Step 2 above corresponds to a random choice of stimulus oscillator, external to the model. Once this oscillator is chosen, the initial conditions for oscillators in Step 3 have a stochastic nature. However, once the initial conditions are selected, the system evolves following a deterministic (albeit nonlinear) set of differential equations, as Step 4. Finally, from the deterministic evolution from stochastic initial conditions, responses are computed in Step 5, and we see in Figure 3 an ensemble of trajectories for the evolution of the relative intensity of a set of oscillators. It is clear from this figure that there is a smearing distribution of computed responses at time 0.2 s. This smearing is smaller than the empirical value reported in Suppes et al. (1964). But this is consistent with the fact that the production of a response by the perceptual and motor system adds additional uncertainty to produce a higher variance of the behavioral smearing distribution.

Reinforcement. Reinforcement of y is neurally described by an oscillator $\varphi_{e,y}$ that couples to the response oscillators with phase relations consistent with the relative intensities of φ_{r_1} and φ_{r_2} producing the response y . The conditioning state of the oscillator system is coded in the couplings between oscillators. Once the reinforcement oscillator is activated, couplings between stimulus and response oscillators change in a way consistent with the reinforced phase relations. For example, if the intensity were greater at φ_{r_2} but we reinforced φ_{r_1} , then the couplings would evolve to push the system toward a closer synchronization with φ_{r_1} . Figure 5 shows the dynamics of oscillators and couplings during an effective reinforcement, and Figure 2 shows the selection of a response for the sampling of the same set of oscillators after the effective reinforcement.

4. Oscillator Model for SR-theory

Now that we have presented the oscillator model from a conceptual point of view, let us look at the mathematical details of the model. As mentioned in (iii) and (v) of Section 2.4, our goal in this paper is to model the stochastic processes described by the random variables \mathbf{X}_n and \mathbf{Z}_n in terms of oscillators. So, let us start with the oscillator computation of a response, corresponding to \mathbf{X}_n . When we think about neural oscillators, we visualize groups of self-sustaining neurons that have some coherence and periodicity in their firing patterns. Here, we assume one of those neural oscillators corresponds to the sampled stimulus s . We will describe below how two neural oscillators r_1 and r_2 can model the computation of randomly selecting response from a continuum of possible responses in accordance with a given probability distribution. A way to approach this is to consider the three harmonic oscillators, s , r_1 , and r_2 , which for simplicity of computation we chose as having the same

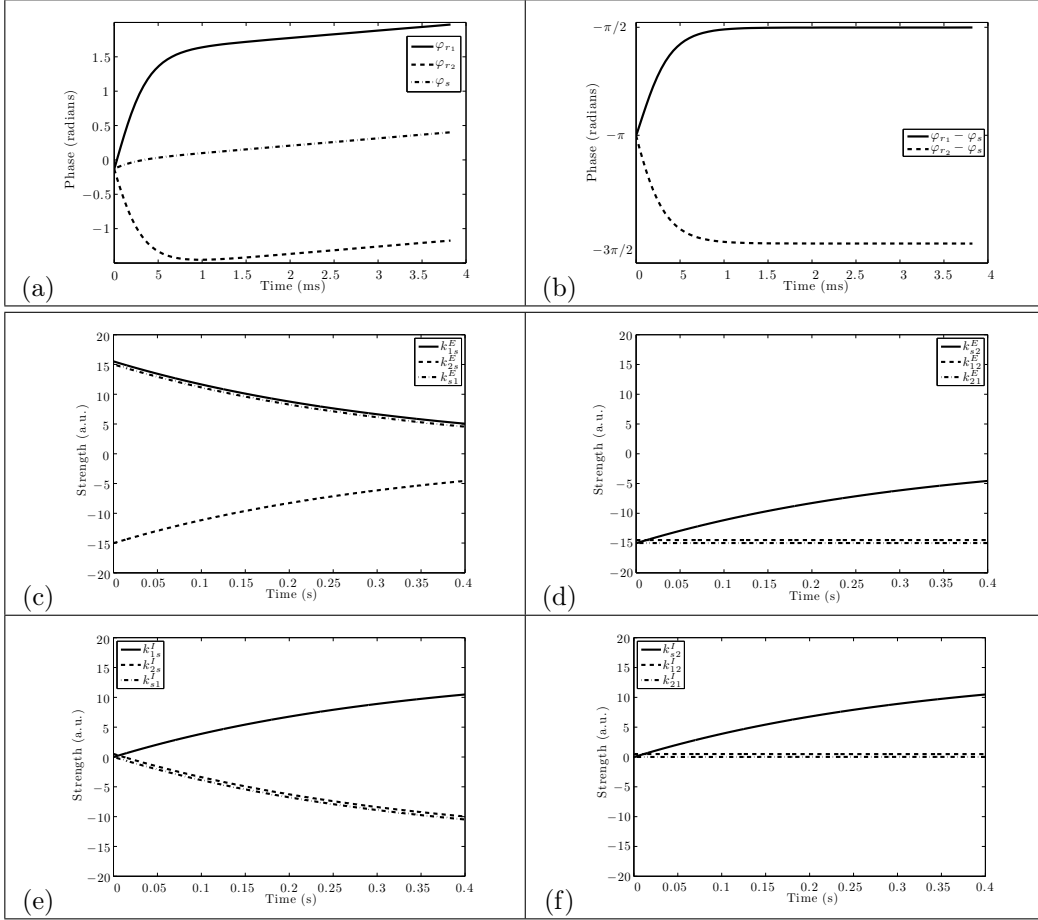


Figure 4: (a) Dynamics of coupled oscillators for the first 6×10^{-3} seconds of reinforcement. Because reinforcement couplings are strong, oscillators quickly converge to an asymptotic state with fixed frequencies and phase relations. Graph (b) shows the quick convergence to the phase relations $-\pi/2$ and $\pi/2$ for r_1 and r_2 with respect to s . Lines in (a) and (b) correspond to the same as Figures 1 and 2. Graphs (c), (d), (e) and (f) show the evolution of the excitatory and inhibitory couplings. Because the system is being reinforced with the phase differences shown in (b), after reinforcement, if the same oscillators are sampled, we should expect a response close to zero in the -1 and 1 scale.

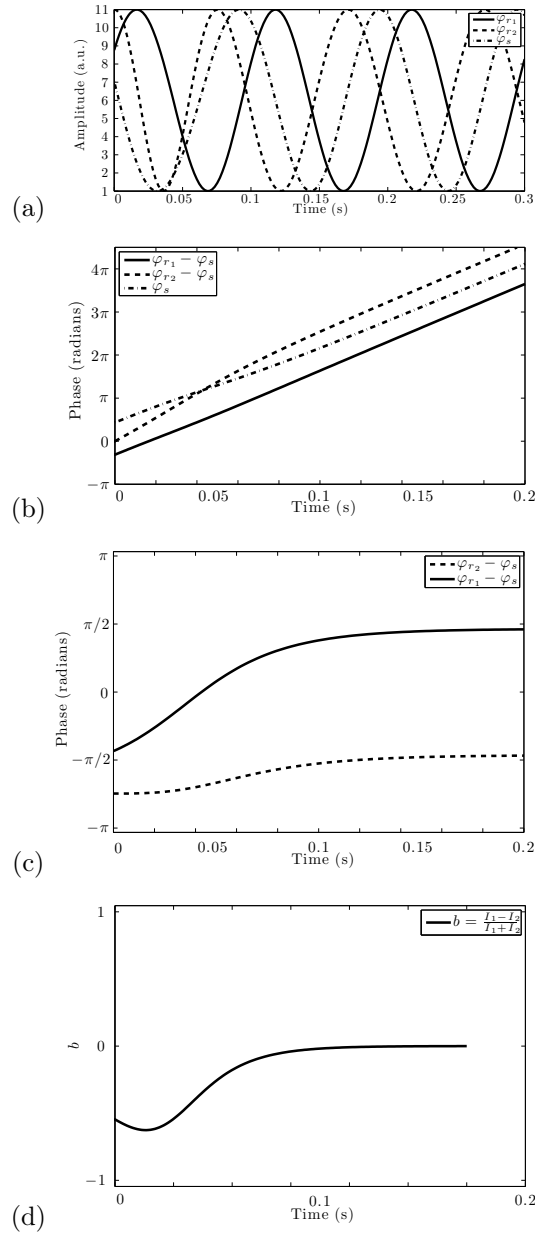


Figure 5: Time evolution of the same oscillators as Figure 2, but now with the new couplings generated after the effective reinforcement shown in Figure 4. Graphs (a) and (b) show the three oscillators, (c) the phase differences, and (d) the response. We see that the response goes to a value close to zero, consistent with the reinforcement of zero.

natural frequency ω_0 and the same amplitude. We write

$$s(t) = A \cos(\omega_0 t) = A \cos(\varphi_s(t)), \quad (15)$$

$$r_1(t) = A \cos(\omega_0 t + \delta\phi_1) = A \cos(\varphi_{r_1}(t)), \quad (16)$$

$$r_2(t) = A \cos(\omega_0 t + \delta\phi_2) = A \cos(\varphi_{r_2}(t)), \quad (17)$$

where $s(t)$, $r_1(t)$, and $r_2(t)$ represent harmonic oscillations, $\varphi_s(t)$, $\varphi_{r_1}(t)$, and $\varphi_{r_2}(t)$ their phases, $\delta\phi_1$ and $\delta\phi_2$ are constants, and A their amplitude. Notice that, since all oscillators have the same amplitude, their dynamics is completely described by their phases. Since neural oscillators have a wave-like behavior (Nunez and Srinivasan, 2006), their dynamics satisfy the principle of superposition, thus making oscillators prone to interference effects. As such, the mean intensity, as usually defined for oscillators, give us a measure of the excitation carried by the oscillations. The mean intensity I_1 is the superposition of $s(t)$ and $r_1(t)$, or

$$\begin{aligned} I_1 &= \left\langle (s(t) + r_1(t))^2 \right\rangle_t \\ &= \left\langle s(t)^2 \right\rangle_t + \left\langle r_1(t)^2 \right\rangle_t + \left\langle 2s(t)r_1(t) \right\rangle_t, \end{aligned}$$

where $\langle \rangle_t$ is the time average. A quick computation gives

$$I_1 = A^2 (1 + \cos(\delta\phi_1)),$$

and, similarly for I_2 ,

$$I_2 = A^2 (1 + \cos(\delta\phi_2)).$$

Therefore, the intensity depends on the phase difference between the response-computation oscillators and the stimulus oscillator.

Let us call I_1^L and I_2^L the intensities after learning. The maximum intensity of I_1^L and I_2^L is $2A^2$, whereas their minimum intensity is zero. Thus, the maximum difference between these intensities happens when their relative phases are such that one of them has a maximum and the other a minimum. For example, if we choose $\delta\phi_1 = 0$ and $\delta\phi_2 = \pi$, then $I_{1,max}^L = A^2 (1 + \cos(0)) = 2A^2$ and $I_{2,min}^L = A^2 (1 + \cos(\pi)) = 0$. Alternatively, if we choose $\delta\phi_1 = \pi$ and $\delta\phi_2 = 0$, $I_{1,min}^L = A^2 (1 + \cos(\pi)) = 0$ and $I_{2,max}^L = A^2 (1 + \cos(0)) = 2A^2$. However, this maximum contrast should only happen when the oscillator learned a clear response, say the one associated with oscillator $r_1(t)$. When we have in-between responses, we should expect less contrast, with the minimum happening when the response lies on the mid-point of the continuum between the responses associated to $r_1(t)$ and $r_2(t)$. This happens if we impose

$$\delta\phi_1 = \delta\phi_2 + \pi \equiv \delta\phi, \quad (18)$$

which results in

$$I_1^L = A^2 (1 + \cos(\delta\phi)), \quad (19)$$

and

$$I_2^L = A^2 (1 - \cos(\delta\phi)). \quad (20)$$

From equations (19) and (20), let $b \in [-1, 1]$ be the normalized difference in intensities between r_1 and r_2 , i.e.

$$b \equiv \frac{I_1^L - I_2^L}{I_1^L + I_2^L} = \cos(\delta\phi), \quad (21)$$

$0 \leq \delta\phi \leq \pi$. So, in principle we can use arbitrary phase differences between oscillators to code for a continuum of responses between -1 and 1 (more precisely, because $\delta\phi$ is a phase, the interval is in the unit circle \mathbb{T} , and not in a compact interval in \mathbb{R}). For arbitrary intervals (ζ_1, ζ_2) , all that is required is a re-scaling of b .

We now turn to the mathematical description of these qualitative ideas. As we saw, we are assuming that the dynamics is encoded by the phases in equations (15)–(17). We assume that stimulus and response-computation neural oscillators have natural frequencies ω_0 , such that their phases are $\varphi(t) = \omega_0 t + \text{constant}$, when they are not interacting with other oscillators. The assumption of the same frequency for stimulus and response-computation oscillators is not necessary, as oscillators with different natural frequency can entrain (Kuramoto, 1984), but it simplifies our analysis, as we focus on phase locking. In real biological systems, we should expect different neural oscillators to have different frequencies. We also assume that they are (initially weakly) coupled to each other with symmetric couplings. The assumption of coupling between the two response-computation oscillators r_1 and r_2 is a detailed feature that has no direct correspondence in the SR model. We are also not requiring the couplings between oscillators to be weak after learning, as learning should usually lead to the strengthening of couplings. This should be contrasted with the usual requirements of weak couplings in the Kuramoto model (Kuramoto, 1984).

At the beginning of a trial, a stimulus is sampled, and its corresponding oscillator, s_j , along with r_1 and r_2 , are activated. The sampling of a stimulus is a stochastic process represented in SR theory by the random variable \mathbf{S}_n , but we do not attempt to model it in detail from neural oscillators. Instead, we just assume that the activation of the oscillators happens in a way consistent with SR theory; a more detailed model of activation that includes such sampling would be desirable, but goes beyond the scope of this paper. Once the stimulus and response-computation oscillators are activated, the phase of each oscillator resets according to a normal distribution centered on zero, i. e., $\bar{\varphi} = 0$, with standard deviation σ_φ , which we here assume is the same for all stimulus and response-computation oscillators. (We choose $\bar{\varphi} = 0$ without loss of generality, since only phase differences are physically meaningful. A Gaussian is used to represent biological variability. A possible mechanism for this phase reset can be found in Wang (1995).) Let $t_{s,n}$ be the time at which the stimulus oscillator is activated on trial n , and let Δt_r be the average amount of time it takes for a response to be selected by oscillators r_1 and r_2 . We use Δt_r as a parameter that is estimated from the experiments, but we believe that more detailed future models should be able to predict the value of Δt_r from the dynamics. Independently of n , the probability density for the phase at time $t_{s,n}$ is given by

$$f(\varphi_i) = \frac{1}{\sigma_\varphi \sqrt{2\pi}} \exp\left(-\frac{\varphi_i^2}{2\sigma_\varphi^2}\right), \quad (22)$$

where $i = s_j, r_1, r_2$. After the stimulus is sampled, the active oscillators evolve for the time interval Δt_r according to the following set of differential equations, known as the Kuramoto equations (Hoppensteadt and Izhikevich, 1996a,b; Kuramoto, 1984).

$$\frac{d\varphi_i}{dt} = \omega_i - \sum_{i \neq j} k_y \sin(\varphi_i - \varphi_j + \delta_{ij}), \quad (23)$$

where k_y is the coupling constant between oscillators i and j , and δ_{ij} is an anti-symmetric matrix representing the phase differences we wish to code, and i and j can be either s , r_1 , or r_2 .

For N stimulus oscillators s_j , $j = 1, \dots, N$, we may now rewrite (23) for the special case of the three oscillator equations for s_j , r_1 , and r_2 . We introduce in these equation notation for excitatory (k_j^E) and inhibitory (k_j^I) couplings. These are the $4N$ excitatory and inhibitory coupling strengths between oscillators (a more detailed explanation of how (24)–(26) are obtained from (23), as well as

the physical interpretation of the coefficients $k_{s_1, r_1}^I, \dots, k_{s_N, r_2}^E, k_{r_1, r_2}^E$ can be found in subsection 4.2).

$$\begin{aligned} \frac{d\varphi_{s_j}}{dt} &= \omega_0 - k_{s_j, r_1}^E \sin(\varphi_{s_j} - \varphi_{r_1}) \\ &\quad - k_{s_j, r_2}^E \sin(\varphi_{s_j} - \varphi_{r_2}) \\ &\quad - k_{s_j, r_1}^I \cos(\varphi_{s_j} - \varphi_{r_1}) \\ &\quad - k_{s_j, r_2}^I \cos(\varphi_{s_j} - \varphi_{r_2}), \end{aligned} \tag{24}$$

$$\begin{aligned} \frac{d\varphi_{r_1}}{dt} &= \omega_0 - k_{r_1, s_j}^E \sin(\varphi_{r_1} - \varphi_{s_j}) \\ &\quad - k_{r_1, r_2}^E \sin(\varphi_{r_1} - \varphi_{r_2}) \\ &\quad - k_{r_1, s_j}^I \cos(\varphi_{r_1} - \varphi_{s_j}) \\ &\quad - k_{r_1, r_2}^I \cos(\varphi_{r_1} - \varphi_{r_2}), \end{aligned} \tag{25}$$

$$\begin{aligned} \frac{d\varphi_{r_2}}{dt} &= \omega_0 - k_{r_2, s_j}^E \sin(\varphi_{r_2} - \varphi_{s_j}) \\ &\quad - k_{r_2, r_1}^E \sin(\varphi_{r_2} - \varphi_{r_1}) \\ &\quad - k_{r_2, s_j}^I \cos(\varphi_{r_2} - \varphi_{s_j}) \\ &\quad - k_{r_2, r_1}^I \cos(\varphi_{r_2} - \varphi_{r_1}), \end{aligned} \tag{26}$$

where φ_{s_j} , φ_{r_1} , and φ_{r_2} are their phases, ω_0 their natural frequency. Equations (24)–(26) usually contain the amplitudes of the oscillators as a coupling factor. For example, instead of just k_{s_j, r_1}^E in (24), the standard form of Kuramoto’s equation would have a $A_{s_j} A_{r_1} k_{s_j, r_1}^E$ term multiplying $\sin(\varphi_{s_j} - \varphi_{r_1})$ (Kuramoto, 1984). For simplicity, we omit this term, as it can be absorbed by k_{s_j, r_1}^E if the amplitudes are unchanged. Before any conditioning, the values for the coupling strengths are chosen following a normal distribution $g(k)$ with mean \bar{k} and standard deviation σ_k . It is important to note that reinforcement will change the couplings while the reinforcement oscillator is acting upon the stimulus and response oscillators, according to the set of differential equations presented later in this section. The solutions to (24)–(26) and the initial conditions randomly distributed according to $f(\varphi_i)$ give us the phases at time $t_{r, n} = t_{s, n} + \Delta t_r$. (Making Δt_r a random variable rather than a constant is a realistic generalization of the constant value we have used in computations.) The coupling strengths between oscillators determine their phase locking and how fast it happens.

4.1. Oscillator Dynamics of Learning from Reinforcement

The dynamics of couplings during reinforcement, corresponding to changes in the conditioning $\mathbf{Z}_{s, n}$. A reinforcement is a strong external learning event that drives all active oscillators to synchronize with frequency ω_e to the reinforcement oscillator, while phase locking to it. We choose $\omega_e \neq \omega_0$ to keep its role explicit in our computations. In (24)–(26) there is no reinforcement, and as we noted earlier, prior to any reinforcement, the couplings $k_{s_1, r_1}^I, \dots, k_{s_N, r_2}^E$ are normally distributed with mean \bar{k} and standard deviation σ_k . To develop equations for conditioning, we assume that when reinforcement is effective, the reinforcement oscillator deterministically interferes with the evolution of the other oscillators. This is done by assuming that the reinforcement event forces the reinforced response-computation and stimulus oscillators to synchronize with the same phase difference of $\delta\varphi$, while the two response-computation oscillators are kept synchronized with a phase difference of π . Let the reinforcement oscillator be activated on trial n at time $t_{e, n}$, $t_{r, n+1} > t_{e, n} > t_{r, n}$, during an interval Δt_e . Let K_0 be the coupling strength between the reinforcement oscillator and the stimulus and response-computation oscillators. In order to match the probabilistic SR axiom governing the effectiveness of reinforcement, we assume, as something beyond Kuramoto’s equations, that there is a normal probability distribution governing the coupling strength K_0 between the reinforcement and

the other active oscillators. It has mean \overline{K}_0 and standard deviation σ_{K_0} . Its density function is:

$$f(K_0) = \frac{1}{\sigma_{K_0} \sqrt{2\pi}} \exp \left\{ -\frac{1}{2\sigma_{K_0}^2} (K_0 - \overline{K}_0)^2 \right\}. \quad (27)$$

As already remarked, a reinforcement is a disruptive event. When it is effective, all active oscillators phase-reset at $t_{e,n}$, and during reinforcement the phases of the active oscillators evolve according to the following set of differential equations.

$$\begin{aligned} \frac{d\varphi_{s_j}}{dt} &= \omega_0 - k_{s_j, r_1}^E \sin(\varphi_{s_j} - \varphi_{r_1}) \\ &\quad - k_{s_j, r_2}^E \sin(\varphi_{s_j} - \varphi_{r_2}) \\ &\quad - k_{s_j, r_1}^I \cos(\varphi_{s_j} - \varphi_{r_1}) \\ &\quad - k_{s_j, r_2}^I \cos(\varphi_{s_j} - \varphi_{r_2}) \\ &\quad - K_0 \sin(\varphi_{s_j} - \omega_e t), \end{aligned} \quad (28)$$

$$\begin{aligned} \frac{d\varphi_{r_1}}{dt} &= \omega_0 - k_{r_1, s_j}^E \sin(\varphi_{r_1} - \varphi_{s_j}) \\ &\quad - k_{r_1, r_2}^E \sin(\varphi_{r_1} - \varphi_{r_2}) \\ &\quad - k_{r_1, s_j}^I \cos(\varphi_{r_1} - \varphi_{s_j}) \\ &\quad - k_{r_1, r_2}^I \cos(\varphi_{r_1} - \varphi_{r_2}) \\ &\quad - K_0 \sin(\varphi_{r_1} - \omega_e t - \delta\varphi), \end{aligned} \quad (29)$$

$$\begin{aligned} \frac{d\varphi_{r_2}}{dt} &= \omega_0 - k_{r_2, s_j}^E \sin(\varphi_{r_2} - \varphi_{s_j}) \\ &\quad - k_{r_2, r_1}^E \sin(\varphi_{r_2} - \varphi_{r_1}) \\ &\quad - k_{r_2, s_j}^I \cos(\varphi_{r_2} - \varphi_{s_j}) \\ &\quad - k_{r_2, r_1}^I \cos(\varphi_{r_2} - \varphi_{r_1}) \\ &\quad - K_0 \sin(\varphi_{r_2} - \omega_e t - \delta\varphi + \pi). \end{aligned} \quad (30)$$

The excitatory couplings are reinforced if the oscillators are in phase with each other, according to the following equations.

$$\frac{dk_{s_j, r_1}^E}{dt} = \epsilon(K_0) \left[\alpha \cos(\varphi_{s_j} - \varphi_{r_1}) - k_{s_j, r_1}^E \right], \quad (31)$$

$$\frac{dk_{s_j, r_2}^E}{dt} = \epsilon(K_0) \left[\alpha \cos(\varphi_{s_j} - \varphi_{r_2}) - k_{s_j, r_2}^E \right], \quad (32)$$

$$\frac{dk_{r_1, r_2}^E}{dt} = \epsilon(K_0) \left[\alpha \cos(\varphi_{r_1} - \varphi_{r_2}) - k_{r_1, r_2}^E \right], \quad (33)$$

$$\frac{dk_{r_1, s_j}^E}{dt} = \epsilon(K_0) \left[\alpha \cos(\varphi_{s_j} - \varphi_{r_1}) - k_{r_1, s_j}^E \right], \quad (34)$$

$$\frac{dk_{r_2, s_j}^E}{dt} = \epsilon(K_0) \left[\alpha \cos(\varphi_{s_j} - \varphi_{r_2}) - k_{r_2, s_j}^E \right], \quad (35)$$

$$\frac{dk_{r_2, r_1}^E}{dt} = \epsilon(K_0) \left[\alpha \cos(\varphi_{r_1} - \varphi_{r_2}) - k_{r_2, r_1}^E \right]. \quad (36)$$

Similarly, for inhibitory connections, if two oscillators are perfectly off sync, then we have a reinforcement of the inhibitory connections.

$$\frac{dk_{s_j, r_1}^I}{dt} = \epsilon(K_0) \left[\alpha \sin(\varphi_{s_j} - \varphi_{r_1}) - k_{s_j, r_1}^I \right], \quad (37)$$

$$\frac{dk_{s_j, r_2}^I}{dt} = \epsilon(K_0) \left[\alpha \sin(\varphi_{s_j} - \varphi_{r_2}) - k_{s_j, r_2}^I \right], \quad (38)$$

$$\frac{dk_{r_1, r_2}^I}{dt} = \epsilon(K_0) \left[\alpha \sin(\varphi_{r_1} - \varphi_{r_2}) - k_{r_1, r_2}^I \right], \quad (39)$$

$$\frac{dk_{r_1, s_j}^I}{dt} = \epsilon(K_0) \left[\alpha \sin(\varphi_{r_1} - \varphi_{s_j}) - k_{r_1, s_j}^I \right], \quad (40)$$

$$\frac{dk_{r_2, s_j}^I}{dt} = \epsilon(K_0) \left[\alpha \sin(\varphi_{r_2} - \varphi_{s_j}) - k_{r_2, s_j}^I \right], \quad (41)$$

$$\frac{dk_{r_2, r_1}^I}{dt} = \epsilon(K_0) \left[\alpha \sin(\varphi_{r_2} - \varphi_{r_1}) - k_{r_2, r_1}^I \right]. \quad (42)$$

In the above equations,

$$\epsilon(K_0) = \begin{cases} 0 & \text{if } K_0 < K' \\ \epsilon_0 & \text{otherwise,} \end{cases} \quad (43)$$

where $\epsilon_0 \ll \omega_0$, α and K_0 are constant during Δt_e (Hoppensteadt and Izhikevich, 1996a,b), and K' is a threshold constant throughout all trials. The function $\epsilon(K_0)$ represents nonlinear effects in the brain. These effects could be replaced by the use of a sigmoid function $\epsilon_0(1 + \exp\{-\gamma(K_0 - K')\})^{-1}$ (Eeckman and Freeman, 1991) in (31)–(42), but we believe that our current setup makes the probabilistic features clearer. In both cases, we can think of K' as a threshold below which the reinforcement oscillator has no (or very little) effect on the stimulus and response-computation oscillators.

Before we proceed, let us analyze the asymptotic behavior of these equations. From (31)–(42) and with the assumption that K_0 is very large, we have, once we drop the terms that are small compared to K_0 ,

$$\frac{d\varphi_{s_j}}{dt} \approx \omega_o - K_0 \sin(\varphi_{s_j} - \omega_e t), \quad (44)$$

$$\frac{d\varphi_{r_1}}{dt} \approx \omega_o - K_0 \sin(\varphi_{r_1} - \omega_e t - \delta\varphi), \quad (45)$$

$$\frac{d\varphi_{r_2}}{dt} \approx \omega_o - K_0 \sin(\varphi_{r_2} - \omega_e t - \delta\varphi + \pi). \quad (46)$$

It is straightforward to show that the solutions for (44)–(46) converge, for $t > 2/\sqrt{K_0^2 - (\omega_e - \omega_0)^2}$ and $K_0^2 \gg (\omega_0 - \omega_e)^2$, to $\varphi_{s_j} = \varphi_{r_1} = \omega_e t - \pi$ and $\varphi_{r_2} = \omega_e t$ if $\omega_e \neq \omega_0$. So, the effect of the new terms added to Kuramoto's equations is to force a specific phase synchronization between s_j , r_1 , and r_2 , and the activated reinforcement oscillator. This leads to the fixed points $\varphi_s = \omega_e t$, $\varphi_{r_1} = \omega_e t + \delta\varphi$, $\varphi_{r_2} = \omega_e t + \delta\varphi - \pi$. With this reinforcement, the excitatory couplings go to the following asymptotic values $k_{s, r_1}^E = k_{r_1, s}^E = -k_{s, r_2}^E = -k_{r_2, s}^E = \alpha \cos(\delta\varphi)$, $k_{r_1, r_2}^E = k_{r_2, r_1}^E = -\alpha$, and the inhibitory ones go to $k_{s, r_1}^I = -k_{r_1, s}^I = -k_{s, r_2}^I = k_{r_2, s}^I = \alpha \sin(\delta\varphi)$, and $k_{r_1, r_2}^I = k_{r_2, r_1}^I = 0$. We show in Appendix A that these couplings lead to the desired stable fixed points corresponding to the phase differences $\delta\varphi$.

We now turn our focus to equations (31)–(42). For simplicity, we will consider the case where $\delta\varphi = 0$ is reinforced. For $K_0 > K'$, φ_{s_j} and φ_{r_1} evolve, approximately, to $\omega_e t + \pi$, and φ_{r_2} to $\omega_e t$. Thus, some couplings in (31)–(42) tend to a solution of the form $\alpha + c_1 \exp(-\epsilon_0 t)$, whereas others tend to $-\alpha + c_2 \exp(-\epsilon_0 t)$, with c_1 and c_2 being integration constants. For a finite time $t > 1/\epsilon_0$, depending on the couplings, the values satisfy the stability requirements shown above.

The phase differences between stimulus and response oscillators are determined by which reinforcement is driving the changes to the couplings during learning. From (31)–(42), reinforcement may be

effective only if $\Delta t_e > \epsilon_0^{-1}$ (see Seliger et al. (2002) and Appendix A.6), setting a lower bound for ϵ_0 , as Δt_e is fixed by the experiment. For values of $\Delta t_e > \epsilon_0^{-1}$, the behavioral probability parameter θ of effective reinforcement is, from (27) and (43), reflected in the equation:

$$\theta = \int_{K'}^{\infty} f(K_0) dK_0. \quad (47)$$

This relationship comes from the fact that if $K_0 < K'$, there is no effective learning from reinforcement, since there are no changes to the couplings due to (31)–(42), and (24)–(26) describe the oscillators' behavior (more details can be found in Appendix A). Intuitively K' is the effectiveness parameter. The larger it is, relative to \overline{K}_0 , the smaller the probability the random value K_0 of the coupling will be effective in changing the values of the couplings through (31)–(42).

Equations (31)–(42) are similar to the evolution equations for neural networks, derived from some reasonable assumptions in Hoppensteadt and Izhikevich (1996a,b). The general idea of oscillator learning similar to (31)–(42) was proposed in Seliger et al. (2002) and Nishii (1998) as possible learning mechanisms.

Thus, a modification of Kuramoto's equations, where we include asymmetric couplings and inhibitory connections, permit the coding of any desired phase differences. Learning becomes more complex, as several new equations are necessary to accommodate the lack of symmetries. However, the underlying ideas are the same, i.e., that neural learning happens in a Hebb-like fashion, via the strengthening of inhibitory and excitatory oscillator couplings during reinforcement, which approximates an SR learning curve.

In summary, the coded phase differences may be used to model a continuum of responses within SR theory in the following way. At the beginning of a trial, the oscillators are reset with a small fluctuation, as in the one-stimulus model, according to the distribution (22). Then, the system evolves according to (24)–(26) if no reinforcement is present, and according to (28)–(42) if reinforcement is present. The coupling constants and the conditioning of stimuli are not reset at the beginning of each trial. Because of the finite amount of time for a response, the probabilistic characteristics of the initial conditions lead to the smearing of the phase differences after a certain time, with an effect similar to that of the smearing distribution in the SR model for a continuum of responses (Suppes and Frankmann (1961); Suppes et al. (1964)). We emphasize that the smearing distribution is not introduced as an extra feature of the oscillator model, but comes naturally from the stochastic properties of it.

Oscillator Computations for Two-Response Models. An important case for the SR model is when participants select from a set of two possible responses, a situation much studied experimentally. We can, intuitively, think of this as a particular case where the reinforcement selects from a continuum of responses two well-localized regions, and one response would be any point selected in one region and the other response any point selected on the other region. In our oscillator model, this can be accomplished by reinforcing, say, $\delta\varphi = 0$, thus leading to responses on a continuum that would be localized in a region close to $b = 1$, and small differences between the actual answer and 1 would be considered irrelevant. More accurately, if a stimulus oscillator phase-locks in phase to a response-computation oscillator, this represents in SR theory that the stimulus is conditioned to a response, but we do not require precise phase locking between the stimulus and response-oscillators. The oscillator computing the response at trial n is the oscillator whose actual phase difference at time $t_{r,n}$ is the smaller with respect to s_j , i.e., the smaller c_i ,

$$c_i = \left\lfloor \frac{1}{2\pi} |\varphi_{r_i} - \varphi_{s_j}| \right\rfloor - \left\lfloor \frac{1}{2\pi} |\varphi_{r_i} - \varphi_{s_j}| \right\rfloor - \frac{1}{2}, \quad (48)$$

where $\lfloor x \rfloor$ is the largest integer not greater than x , and $i = 1, 2$.

4.2. Physical Interpretation of Dynamical Equations

A problem with equation (23) is that it does not have a clear physical or neural interpretation. How are the arbitrary phase differences δ_{ij} to be interpreted? Certainly, they cannot be interpreted by

the excitatory firing of neurons, as they would lead to δ_{ij} being either 0 or π , as shown in Appendix A. Furthermore, since the k_{ij} represent oscillator couplings, how are the phase differences stored? To answer these questions, let us rewrite (23) as

$$\begin{aligned} \frac{d\varphi_i}{dt} &= \omega_i - \sum_j k_{ij} \cos(\delta_{ij}) \sin(\varphi_i - \varphi_j) \\ &\quad - \sum_j k_{ij} \sin(\delta_{ij}) \cos(\varphi_i - \varphi_j). \end{aligned} \quad (49)$$

Since the terms involving the phase differences δ_{ij} are constant, we can write (49) as

$$\frac{d\varphi_i}{dt} = \omega_i - \sum_j [k_{ij}^E \sin(\varphi_i - \varphi_j) + k_{ij}^I \cos(\varphi_i - \varphi_j)], \quad (50)$$

where $k_{ij}^E = k_{ij} \cos(\delta_{ij})$ and $k_{ij}^I = k_{ij} \sin(\delta_{ij})$. Equation (23) now has an immediate physical interpretation. Since k_{ij}^E makes oscillators φ_i and φ_j approach each other, as before, we can think of them as corresponding to excitatory couplings between neurons or sets of neurons. When a neuron φ_j fires shortly before it is time for φ_i to fire, this makes it more probable φ_i will fire earlier, thus bringing its rate closer to φ_j . On the other hand, for k_{ij}^I the effect is the opposite: if a neuron in φ_j fires, k_{ij}^I makes the neurons in φ_i fire further away from it. Therefore, k_{ij}^I cannot represent an excitatory connection, but must represent inhibitory ones between φ_i and φ_j . In other words, we may give physical meaning to learning phase differences in equations (23) by rewriting them to include excitatory and inhibitory terms.

We should stress that inhibition and excitation have different meanings in different disciplines, and some comments must be made to avoid confusion. First, here we are using inhibition and excitation in a way analogous to how they are used in neural networks, in the sense that inhibitions decrease the probability of a neuron firing shortly after the inhibitory event, whereas excitation increases this probability. Similarly, the inhibitory couplings in equations (50) push oscillators apart, whereas the excitatory couplings bring them together. However, though inhibitory and excitatory synaptic couplings provide a reasonable model for the couplings between neural oscillators, we are not claiming to have derived equations (50) from such fundamental considerations. In fact, other mechanisms, such as asymmetries of the extracellular matrix or weak electric-field effects, could also yield similar results. The second point is to distinguish our use of inhibition from that in behavioral experiments. In animal experiments, inhibition is usually the suppression of a behavior by negative conditioning (Dickinson, 1980). As such, this concept has no direct analogue in the standard mathematical form of SR theory presented in Section 2. But we emphasize that our use of inhibition in equations (50) is not the behavioral one, but instead closer to the use of inhibition in synaptic couplings.

Before we proceed, another issue needs to be addressed. In a preliminary analysis of the fixed points, we see three distinct possibilities: $\phi_{1j} = \phi_{2j} = 0$, (ii) $\phi_{1j} = \pi$, $\phi_{2j} = 0$, and (iii) $\phi_{1j} = 0$, $\phi_{2j} = \pi$. A detailed investigation of the different fixed points and their stability is given in Appendix A. For typical biological parameters and the physical ones we have added, the rate of convergence is such that the solutions are well approximated by the asymptotic fixed points by the time a response is made. But given that we have three different fixed points, how can r_1 be the conditioned response computation oscillator (fixed point iii) if r_2 can also phase-lock in phase (fixed point ii)? To answer this question, we examine the stability of these fixed points, i.e., whether small changes in the initial conditions for the phases lead to the same phase differences. In Appendix A we linearize for small fluctuations around each fixed point. As shown there (Equation Appendix A.81), a sufficient condition for fixed point $(0, \pi)$ to be stable is

$$k_{s_j, r_2} k_{r_1, r_2} > k_{s_j, r_1} k_{s_j, r_2} + k_{s_j, r_1} k_{r_1, r_2},$$

and the other fixed points are unstable (see Fig. 6 below); similar results can be computed for the other fixed points. It is important to notice that, although the above result shows stability, it does not imply synchronization within some fixed finite time. Because neural oscillators need to operate in rather small amounts of time, numerical simulations are necessary to establish synchronization in an appropriately short amount of time (though some arguments are given in Appendix A.4 with respect to the time of convergence and the values of the coupling constants). If the couplings are zero, the

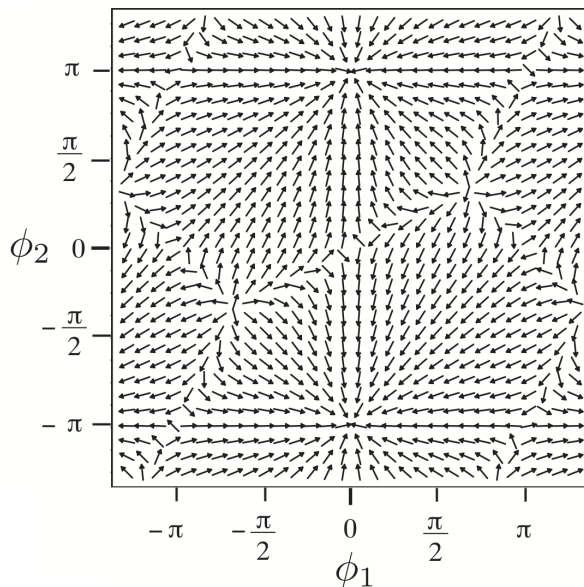


Figure 6: Field plot, generated using Maple 10, for couplings $k_{s_j, r_1} = k_{r_1, r_2} = -k$ and $k_{s_j, r_2} = k$, $k > 0$. Field lines show that the fixed point at $(0, \pi)$ is stable, whereas $(0, 0)$, $(\pi, 0)$, (π, π) , $(\pi/3, 2\pi/3)$, and $(2\pi/3, \pi/3)$ are unstable. Thus, for a randomly selected initial condition, in a finite amount of time s_j approaches the phase of r_1 and departs from r_2 .

model still picks one of the oscillators: the one with the minimum value for c_i in (48). But in this case, because of the small fluctuations in the initial conditions, the probability for each response is $1/2$, as expected, corresponding, obviously, to the SR parameter $p = 1/2$ in the one-stimulus model.

4.3. Parameter values

We turn now to the parameters used in the oscillator models. In the above equations, we have as parameters N , ω_0 , ω_e , α , Δt_r , Δt_e , \bar{k} , σ_k , $\bar{\varphi}$, σ_φ , ϵ_0 , \bar{K}_0 , σ_{K_0} , and K' . This large number of parameters stands in sharp contrast to the small number needed for SR theory, which is abstract and therefore much simpler. In our view, any other detailed physical model of SR theory will face a similar problem. Experimental evidence constrains the range of values for ω_0 , ω_e , Δt_r , and Δt_e , and throughout this paper we choose ω_0 and ω_e to be at the order of 10 Hz, $\Delta t_r = 200$ ms, and $\Delta t_e = 400$ ms. These natural frequencies were chosen because: (i) they are in the lower range of frequencies measured for neural oscillators (Freeman and Barrie, 1994; Friedrich et al., 2004; Kazantsev et al., 2004; Murthy and Fetz, 1992; Suppes and Han, 2000; Tallon-Baudry et al., 2001), and the lower the frequency, the longer the time it takes for two oscillators to synchronize, which imposes a lower bound on the time taken to make a response, (ii) data from Suppes et al. (1997, 1998, 1999b,a); Suppes and Han (2000) suggest that most frequencies used for the brain representation of language are close to 10 Hz, and (iii)

choosing a small range of frequencies simplifies the oscillator behavior.² We use $\Delta t_r = 200$ ms, which is consistent with the part it plays in the behavioral response times in many psychological experiments; for extended analysis of the latter see Luce (1986). The value for $\Delta t_e = 400$ ms is also consistent with psychological experiments.

Before any conditioning, we should not expect the coupling strengths between oscillators to favor one response over the other, so we set $\bar{k} = 0$ Hz. The synchronization of oscillators at the beginning of each trial implies that their phases are almost the same, so for convenience we use $\bar{\varphi} = 0$. The standard deviations σ_k and σ_φ are not directly measured, and we use for our simulations the reasonable values of $\sigma_k = 10^{-3}$ Hz and $\sigma_\varphi = \pi/4$ Hz. Those values were chosen because σ_k should be very small, since it is related to neuronal connections before any conditioning, and σ_φ should allow for a measurable phase reset at the presentation of a stimulus, so $\sigma_\varphi < 1$.

The values of α , ϵ_0 , \bar{K}_0 , and σ_{K_0} are based on theoretical considerations. As we discussed in the previous paragraph, \bar{K}_0 is the mean strength for the coupling of the reinforcement oscillator, and σ_{K_0} is the standard deviation of its distribution. We assume in our model that this strength is constant during a trial, but that it varies from trial to trial according to the given probability distribution. The parameter α is related to the maximum strength allowed for the coupling constants k_{s_j, r_1} , k_{s_j, r_2} , and k_{r_1, r_2} . Because of the stability conditions for the fixed points, shown above, any value of α leads to phase locking, given enough time. The magnitude of α is monotonically related to how fast the system phase locks. It needs to be at least of the order of $1/\Delta t_r$ if the oscillators are to phase lock within the behavioral response latency. Another important parameter is ϵ_0 , and we can see its role by fixing the phases and letting the system evolve. In this situation, the couplings converge exponentially to α with a characteristic time ϵ_0^{-1} , so ϵ_0 determines how fast the couplings change. The time of response, Δt_r , given experimentally, sets a minimum value of 5 Hz for α , since $\alpha > \Delta t_r^{-1} = 5$ Hz is needed to have phase locking from Kuramoto-type equations. The time of reinforcement, Δt_e , and natural frequency ω_0 are related to ϵ_0 by $\epsilon_0 > \Delta t_e^{-1} = 2.5$ Hz and $\epsilon_0 \ll \omega_0$. Finally, to have an effective reinforcement, K_0 must satisfy $K_0 \gg \omega_0$. These theoretical considerations are consistent with the values $\alpha = 10$ Hz, $\epsilon_0 = 3$ Hz, $\bar{K}_0 = 4,000$ Hz, and $\sigma_{K_0} = 1,000$ Hz. We note one distinction about the roles of the three probability distributions introduced. Samples are drawn of phases φ and reinforcement oscillator coupling strength K_0 on each trial, but oscillator couplings $k_{s_1, r_1}^E, \dots, k_{s_N, r_2}^I, k_{r_1, r_2}^I$ are sampled only once at the beginning of a simulated experiment and then evolve according to (31)–(42).

Table 1 summarizes the fixed parameter values used in our simulations, independent of considering

Table 1: Fixed values of parameters used to fit the oscillator models to SR experiments.

Parameter	Value	Parameter	Value
α	10 Hz	σ_φ	$\pi/4$
ω_0	10 Hz	\bar{k}	0 Hz
ω_e	12 Hz	σ_k	10^{-3} Hz
Δt_r	200 ms	σ_{K_0}	1,000 Hz
Δt_e	400 ms	\bar{K}_0	4,000 Hz
$\bar{\varphi}$	0	ϵ_0	3 Hz

the experimental design or data of a given SR experiment. This leaves us with two remaining free parameters to estimate from SR experimental data: the number of stimulus oscillators N and the nonlinear cutoff parameter K' . These two parameters have a straightforward relation to the SR ones. N corresponds to the number of stimuli, and K' is monotonically decreasing with the effectiveness of the reinforcement probability θ , as shown in (47).

²However, we should mention that none of the above references involve reinforcement, though we are working with the assumption that reinforcement events are also represented by frequencies that are within the range suggested by evidence.

Fig. 7 exemplifies the phase-difference behavior of three oscillators satisfying the Kuramoto equations. In the figure, as shown, all oscillators start with similar phases, but at 200 ms both s_j and r_1

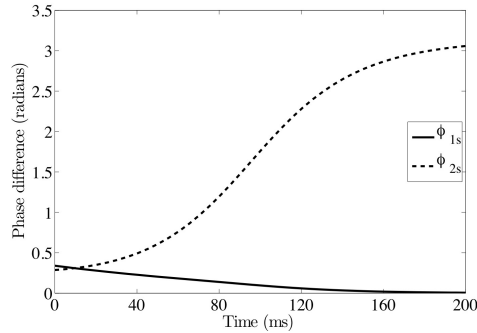


Figure 7: MATLAB computation of the phase differences between three coupled oscillators evolving according to Kuramoto’s equations with couplings $k_{s_j,r_1} = \omega_0 = -k_{s_j,r_2} = k_{r_1,r_2}$ and $\omega_0 = 20\pi \text{ s}^{-1}$ (10 Hz). The solid line represents $\phi_{1s_j} = \varphi_{r_1} - \varphi_{s_j}$, and the dashed $\phi_{2s_j} = \varphi_{r_2} - \varphi_s$.

lock with the same phase, whereas r_2 locks with phase difference π . Details on the theoretical relations between parameters can be found in Appendix A.

5. Comparison with Experiments

Although the oscillator models produce a mean learning curve that fits quite well the one predicted by SR theory, it is well known that stochastic models with underlying assumptions that are qualitatively quite different may predict the same mean learning curves. The asymptotic conditional probabilities, on the other hand, often have very different values, depending on the number N of sampled stimuli assumed. For instance, the observable conditional probability density $j(x_n|y_{n-1}y_{n-2})$ for the one-stimulus model is different from the conditional density for the N -stimulus models, ($N > 1$) as is shown later in this section.

In the following, we compare some behavioral experimental data to such theoretical quantities and to the oscillator-simulation data. We first compare empirical data from an experiment with a continuum of responses to the oscillator-simulation data. Second, we show that in a probability matching experiment (Suppes and Atkinson, 1960, Chapter 10) the experimental and oscillator-simulated data are quite similar and fit rather well to the SR theoretical predications. Finally, we examine the paired-associate learning experiment of Bower (1961), and model it in the same way. Here we focus on the model predictions of stationarity and independence of responses prior to the last error. Again, the original experimental data, and the oscillator-simulation data exhibit these two properties to about the same reasonably satisfactory degree.

5.1. Continuum of Responses

As shown in Section 2, to fit the continuum-of-responses SR model to data, we need to estimate N , the number of stimuli, θ , the probability that a reinforcement is effective, and $K_s(x|z)$, the response smearing distribution of each stimulus s over the set of possible responses. As we saw in Section 3, in the oscillator model θ comes from the dynamics of learning (see equation (47) and corresponding discussion), whereas N is external to the model. The smearing distribution in the oscillator model comes from the stochastic nature of the initial conditions coupled with the nonlinear dynamics of Kuramoto’s equations.

Let us now focus on the experiment, described in Suppes et al. (1964). In it, a screen had a 5-foot diameter circle. A noncontingent reinforcement was given on each trial by a dot of red light on the

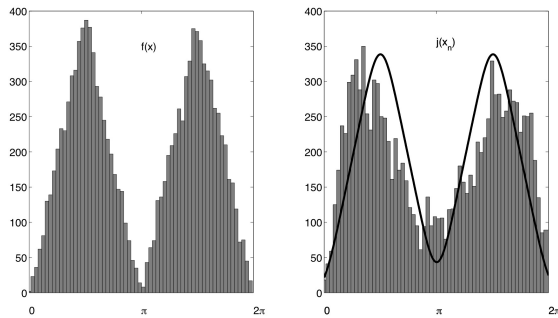


Figure 8: On the left histogram of the reinforcement angles used in the oscillator simulation, and on the right both the SR theoretical density of the one-stimulus model and the histogram of the oscillator-simulated responses.

circumference of the 5-foot circle, with the position determined by a bimodal distribution $f(y)$, given by

$$f(y) = \begin{cases} \frac{2}{\pi^2} y, & 0 \leq x \leq \frac{\pi}{2} \\ \frac{2}{\pi^2} (\pi - y), & \frac{\pi}{2} < x \leq \pi \\ \frac{2}{\pi^2} (y - \pi), & \pi < x \leq \frac{3\pi}{2} \\ \frac{2}{\pi^2} (2\pi - y), & \frac{3\pi}{2} < x \leq 2\pi. \end{cases} \quad (51)$$

At the center of this circle, a knob connected to an invisible shaft allowed the red dot to be projected on the screen at any point on the circle. Participants were instructed to use this knob to predict on each trial the position of the next reinforcement light. The participants were 4 male and 26 female Stanford undergraduates. For this experiment, Suppes et al. (1964) discuss many points related to the predictions of SR theory, including goodness of fit. Here we focus mainly on the relationship between our oscillator-simulated data and the SR predicted conditional probability densities.

Our main results are shown in Figures 8–11. The histograms were computed using the last 400 trials of the 600 trial simulated data for each of the 30 participants, for a total of 12,000 sample points, and b was reparametrized to correspond to the interval $(0, 2\pi)$. The parameters used are the same as those described at the end of Section 4, with the exception of $K'_0 = 4468$, chosen by using equation (47) such that the learning effectiveness of the oscillator model would coincide with the observed value of $\theta = 0.32$ in Suppes et al. (1964). Each oscillator's natural frequency was randomly selected according to a Gaussian distribution centered on 10 Hz, with variance 1 Hz. Figure 8 shows the effects of the smearing distributions on the oscillator-simulated responses. Figure 9 shows the predicted conditional response density $j(x_n|y_{n-1})$ if reinforcement on the previous trial ($n-1$) happened in the interval $(\pi, 3\pi/2)$. As predicted by SR theory, the oscillator-simulated data also exhibit an asymmetric histogram matching the predicted conditional density. We computed from the simulated data the histograms of the conditional distributions $j(x_n|y_{n-1}y_{n-2})$, shown in Figure 10. Finally, if we use our simulated data to generate histograms corresponding to the conditional densities $j(x_n|y_{n-1}x_{n-1})$, we obtain a similar result to that of the one-stimulus model (see Figure 11). We emphasize that, as in the N -stimulus oscillator model used for the paired-associate learning experiment, the continuum-of-response oscillator model can be modified to yield data similar to the statistical predictions of the SR model, if we add oscillators to represent additional stimuli.

Up to now we showed how the oscillator-simulated data compare to the experiments in a tangential way, by fitting them to the predictions of the SR theory, which we know fit the behavioral data rather well. Now we examine how our model performed when we compare directly oscillator-simulated and the behavioral empirical data. For the continuum of responses, we focus on the data presented in Figures 2 and 5 of Suppes et al. (1964), corresponding to our Figures 8 and 9. As the original data are not available anymore, to make a comparison to our simulations we normalized the simulated-data histograms and redrew them with the same number of bins as used in the corresponding figures of Suppes

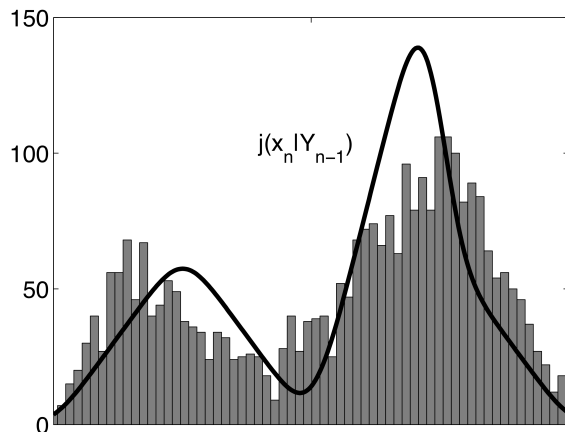


Figure 9: Histogram for the oscillator-simulated response x_n on trial n conditioned to a reinforcement on trial $n - 1$ in the interval $(\pi, 3\pi/2)$. The black line shows the fitted SR theoretical predictions of the one-stimulus model.

et al. (1964). We then performed a two-sample Kolmogorov-Smirnov test to compare the empirical behavioral data with the oscillator-simulated data, the null hypothesis being that the two histograms originated from the same distribution (Keeping, 1995). For the simulated response histogram of Figure 8, the Kolmogorov-Smirnov test yields a p -value of 0.53. So, we cannot reject the null hypothesis, that the simulated data come from the same distribution as the corresponding behavioral data. For the asymmetric conditional probability of Figure 9, the Kolmogorov-Smirnov test yields a p -value of 0.36, once again suggesting that the oscillator simulated data are statistically indistinguishable from the empirical data.

5.2. Experiment on probability matching

The second experiment that we modeled with oscillators is a probability-matching one, described in detail in Suppes and Atkinson (1960, Chapter 10). The experiment consisted of 30 participants, who had to choose between two possible behavioral responses, R_1 or R_2 . A top light on a panel would turn on to indicate to the participant the beginning of a trial. Reinforcement was indicated by a light going on over the correct response key.³ The correct response was noncontingent, with probability $\beta = 0.6$ for reinforcing response R_1 and 0.4 for R_2 . The experiment consisted of 240 trials for each participant.

To compare the oscillator-simulated data with the results for the probability-matching experiment, we first computed, using the behavioral data for the last 100 trials, the log pseudomaximum likelihood function (Suppes and Atkinson, 1960, p. 206)

$$L(\theta, N) = \sum_{i,j,k=1}^2 n_{ij,k} \log P_\infty(R_{k,n+1} | E_{j,n} R_{i,n}),$$

where $n_{ij,k}$ is the observed number of transitions from R_i and E_j on trial n to R_k on trial $n + 1$, and the SR theoretical conditional probabilities $P_\infty(R_{k,n+1} | E_{j,n} R_{i,n})$ are:

³The widely used notation, R_i for response i and E_j for reinforcement j , for experiments with just two responses is followed in describing the second and third experiments.

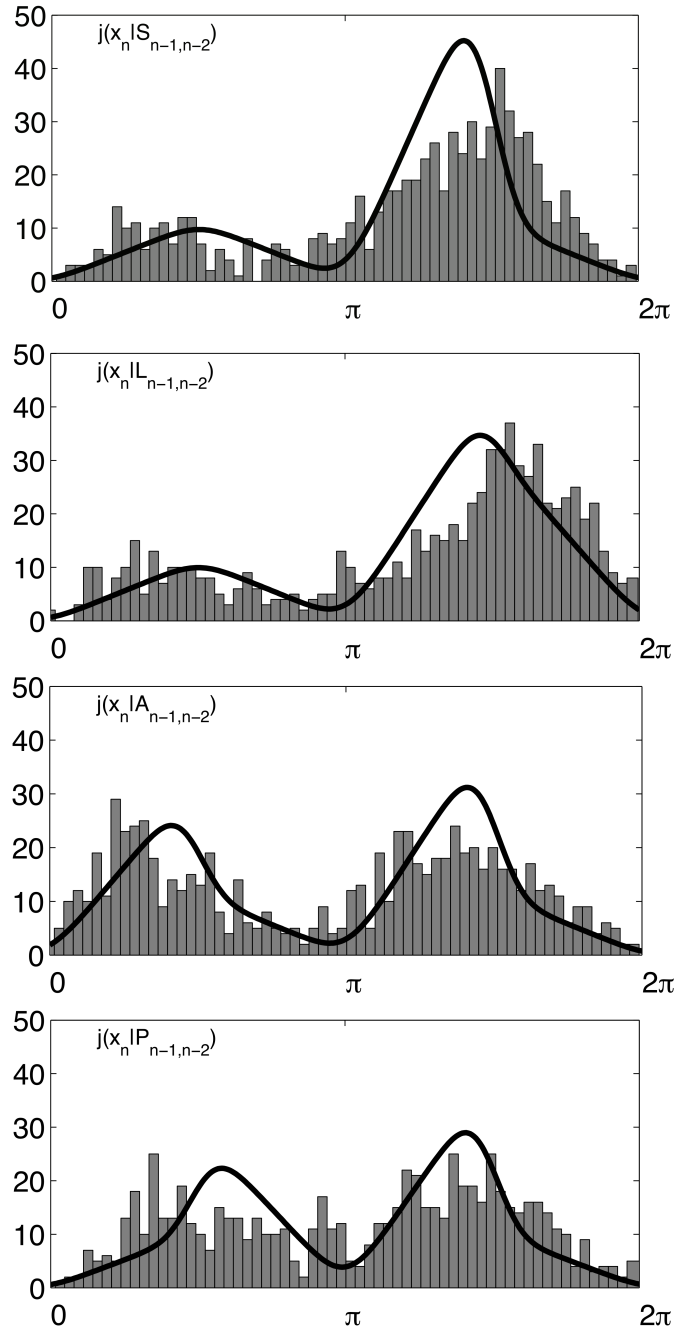


Figure 10: Histograms of oscillators-simulated responses conditioned to reinforcement on the two previous trial. All graphs correspond to simulated responses with reinforcement on trial $n - 1$ being in the interval $(\pi, 3\pi/2)$. S corresponds to reinforcements on trial $n - 2$ occurring in the same interval. L corresponds to reinforcement on $n - 2$ occurring on the interval $(3\pi/2, 2\pi)$, A on the interval $(0, \pi/2)$, and P on $(\pi/2, \pi)$. The solid lines show the SR theoretical one-stimulus model predictions.

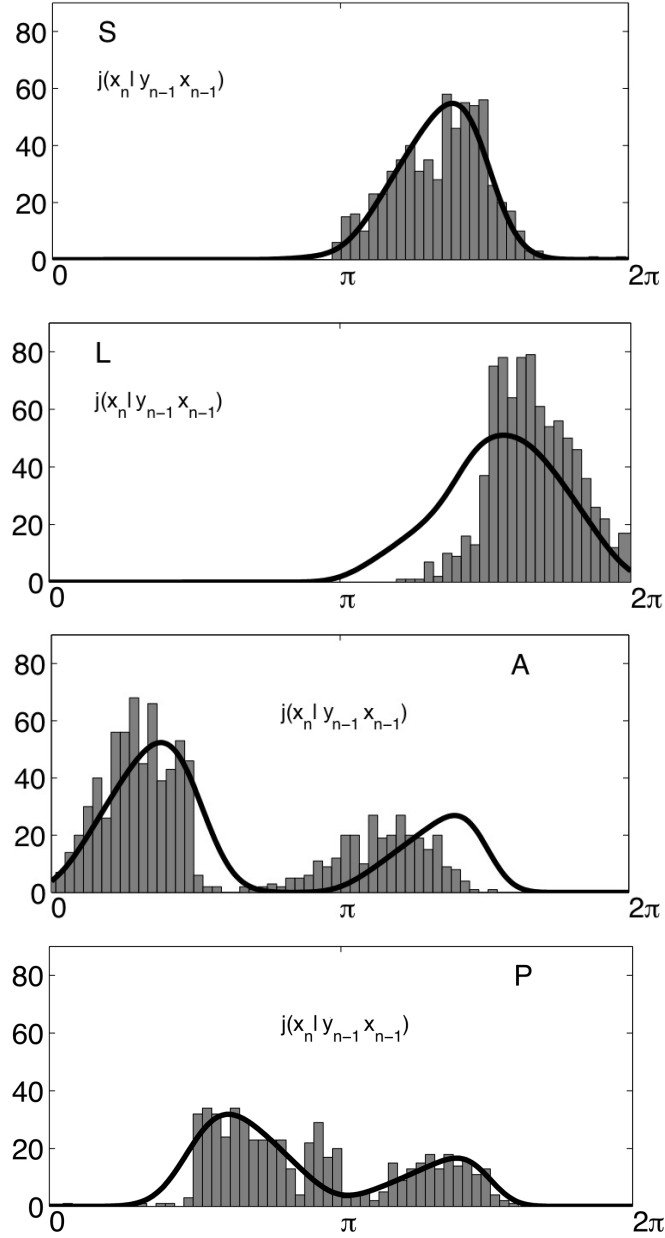


Figure 11: Histograms of oscillators-simulated responses conditioned to reinforcements and simulated responses on the previous trial. All graphs correspond to simulated responses with reinforcement on trial $n - 1$ being in the interval $(\pi, 3\pi/2)$. S corresponds to responses on trial $n - 1$ occurring in the same interval. L corresponds to responses on $n - 1$ occurring in the interval $(3\pi/2, 2\pi)$, A in the interval $(0, \pi/2)$, and P in the interval $(\pi/2, \pi)$. The solid lines are the predictions of the one-stimulus SR model.

$$P_\infty(R_{1,n+1}|E_{1,n}R_{1,n}) = \beta + \frac{1-\beta}{N}, \quad (52)$$

$$P_\infty(R_{1,n+1}|E_{1,n}R_{2,n}) = \beta \left(1 - \frac{1}{N}\right) + \frac{\theta}{N}, \quad (53)$$

$$P_\infty(R_{1,n+1}|E_{2,n}R_{1,n}) = \beta \left(1 - \frac{1}{N}\right) + \frac{1-\theta}{N}, \quad (54)$$

$$P_\infty(R_{1,n+1}|E_{2,n}R_{2,n}) = \beta \left(1 - \frac{1}{N}\right). \quad (55)$$

The log likelihood function $L(\theta, N)$, with $\beta = 0.6$ as in the experiment, had maxima at $\hat{\theta} = 0.600$ for $N = 3$, $\hat{\theta} = 0.631$ for $N = 4$, and $\hat{\theta} = 0.611$ for $\hat{N} = 3.35$, where \hat{N} is the log pseudomaximum likelihood estimate of N (for more details, see Suppes and Atkinson (1960, Chapter 10)). We ran MATLAB oscillator simulations with the same parameters. We computed 240 trials and 30 sets of oscillators, one for each participant, for the three-, and four-stimulus oscillator models. Since the behavioral learning parameter θ relates to K' , we used $K' = 65 \text{ s}^{-1}$ and $K' = 56 \text{ s}^{-1}$ for the three-, and four-stimulus models, respectively, corresponding to $\hat{\theta} = 0.600$, and $\hat{\theta} = 0.631$. Table 2 compares the experimentally observed conditional relative frequencies with the predicted asymptotic values for the $N = 3$ or 4 SR models, and the corresponding oscillator simulations. In Table 2, $P(R_{1,n+1}|E_{1,n}R_{1,n})$ is the asymptotic conditional probability of response R_1 on trial $n + 1$ if on trial n the response was R_1 and the reinforcement was E_1 , and similarly for the other three expressions, for each of the conditions in Table 2, observed frequency, two oscillator simulations and two behavioral predictions.

Table 2: Comparison between experimental results and the corresponding oscillator models. Theoretical results for the N -stimulus model are shown for comparison purposes. The first data row shows experimental values based on the last 100 trials of the 30-subject group. The other rows show the SR theory asymptotic probabilities and simulations for the oscillator models averaged over the last 100 trials. The columns show the asymptotic conditional probabilities. For example, column $R_1|E_1R_1$ shows the asymptotic probability $P(R_1|E_1R_1)$ of response R_1 on trial n given that on trial $n - 1$ the response was R_1 and the reinforcement was E_1 .

	$R_1 E_1R_1$	$R_1 E_1R_2$	$R_1 E_2R_1$	$R_1 E_2R_2$
Observed	.715	.602	.535	.413
Oscillator				
3-stimulus simulation	.705	.574	.522	.381
4-stimulus simulation	.760	.610	.538	.426
SR-theory				
3-stimulus prediction	.733	.600	.533	.400
4-stimulus prediction	.700	.608	.542	.450

In Table 2 we compare the oscillator simulations to the behavioral data and the best fitting asymptotic SR models. Each oscillator model was computed using the same estimated θ value as the corresponding SR model. The fit of the SR model to the empirical data is quite good, as is the fit for the 4-stimulus oscillator model.

5.3. Experiment on paired-associate learning

In this experiment, described in detail in Bower (1961), 29 participants learned a list of ten stimulus items to a criterion of two consecutive errorless cycles. The order of stimulus presentation was randomized for each trial. The visual stimuli were different pairs of consonant letters; the numerical

responses were the numbers 1 or 2, each number being assigned as correct to a randomly selected five stimuli for each participant. A participant was informed of the correct answer following each response. The one-stimulus model fitted the behavioral data the best.

To model with oscillators, we used 29 independent sets of oscillators, each set with ten-stimulus, two-response, and two reinforcements, to reproduce Bower’s setup. For our oscillator simulations we set $N = 1$ and $K' = 94 \text{ s}^{-1}$, $\bar{K}_0 = 90 \text{ Hz}$, and $\sigma_{K_0} = 10 \text{ Hz}$. K' was chosen based on (47) and on Bower’s statistical estimation of the probability of effective reinforcement for the one-stimulus model, which was $\theta = 0.344$.

Bower’s behavioral data were also tested in Suppes and Ginsberg (1963) for the statistical properties of stationarity and independence prior to the last response error, a prediction of the one-stimulus SR model. We compare in Table 3 the behavioral results with those for our oscillator simulation.

Stationarity. The first test is that of stationarity, i.e., whether the probability of a response oscillator phase-locking before the last error is constant. To perform this test, we restricted our oscillator-simulated data set to the M responses that happened *before* the last behavioral error of a given participant. We then divided this set into two, with the first $M/2$ trials being early trials and the remaining $M/2$ late trials. Let n_1 be the number of correct responses in the first half and n_2 the number of correct responses in the second half. If the probability is stationary, then both $n_1/(M/2)$ and $n_2/(M/2)$ should be approximately $(n_1 + n_2)/M$. We used a standard χ^2 test for this null hypothesis of stationarity for the oscillator-simulated responses.

Independence. Restricting ourselves again to trials prior to the last behavioral error, let n_{ij} be the number of transitions from state i to state j , where i and j can take values 0 (correct response) or 1 (incorrect). We use these numbers to estimate the transition probabilities p_{ij} . The null hypothesis of independence is that $p_{00} = p_{10}$ and $p_{01} = p_{11}$. The sample paths used to compute the oscillator

Table 3: Comparison between the paired-associate experimental data and the simulated one-stimulus oscillator data. Notice that N is different for the experiment and the simulation, as N is the number of responses prior to the last error, which varies for each run of the simulations.

	Stationarity
Experiment	$\chi^2 = .97, N = 549,$ $df = 6, p > .95$
Oscillator simulation	$\chi^2 = 2.69, N = 748,$ $df = 6, p > .8$
	Independence
Experiment	$\chi^2 = .97, N = 549,$ $df = 6, p > .95$
Oscillator simulation	$\chi^2 = 0.1, N = 458,$ $df = 6, p > .95$

results in Table 3 were obtained by running simulations in MATLAB 7.1.0.183 (R14), SP 3 with the parameter values given earlier. The simulations consisted of randomly selecting, at each trial, the initial phase according to (22) and then computing phase evolution during Δt_r by numerically solving (24)–(26) using MATLAB’s built-in fourth-fifth order Runge-Kutta method. After Δt_r the phase differences were computed and a response oscillator selected. At the beginning of reinforcement, new initial conditions and a random value for K_0 were drawn according to (22) and (27), respectively. If $K_0 > K'$, then the oscillators’ couplings changed according to (28)–(42), and these equations were numerically solved for the time interval Δt_e also using fourth-fifth order Runge-Kutta, and the new values for the couplings were used on the next trial.

The results in Table 3 show that we cannot sharply differentiate the behavioral and the oscillator-simulation data in testing the null hypotheses of stationarity and independence.

6. Conclusions and Final Remarks

We modeled stimulus-response theory using neural oscillators based on reasonable assumptions from neurophysiology. The effects of the interaction between the neural oscillators were described by phase differences obeying Kuramoto’s equations. Learning was modeled by changes in phases and couplings, driven by a reinforcement oscillator, with phase locking corresponding to behavioral conditioning. We compared the oscillator-simulated data to the data from three behavioral experiments, as well as to the corresponding behavioral-model predictions derived from SR theory. Our simulation results support the claim that neural oscillators may be used to model stimulus-response theory, as well as behavioral experiments testing the theory.

From (47), behavioral and oscillator-simulated data relate the SR conditioning parameter θ to K' , σ_{K_0} , and $\overline{K_0}$. Despite the large number of parameters, our numerical oscillator simulations, all done with the same set of parameters, except N and K' , show that the statistical fit reported in Table 3 and conditional probabilities in Table 2 do not vary much even when these parameters are changed significantly. The most important constraint is this. Once all parameters are fixed then the stimulus-response conditioning parameter θ is a nonlinear monotonically decreasing function of K' given by (47). As our oscillator-simulations are refined and extended to more experiments, further constraints should narrow the parameter space.

As is sometimes remarked, stimulus-response theory abstracts from many necessary processes that must have a physical realization. From a general psychological viewpoint, independent of the details of physical realization, undoubtedly the most obvious missing process is the perceptual recognition of the sampling of the same, or nearly the same stimulus, and of the reinforcement stimulus patterns different on repeated trials. We should be able to expand the present setup to include oscillators that recognize, by similarity or congruence computations, when a sampled stimulus type is one that has been previously sampled. Prior work on pattern recognition will be useful here. Our own earlier experimental work on computational models that recognize auditory or visual word, sentence or other brain images, such as those of red triangles or blue circles, provides substantial evidence that a single oscillator with one given natural frequency will be inadequate. Multiple oscillators with different natural frequencies will be required for such similarity recognition. For examples of such computational models applied to EEG-recorded brain data, see Suppes et al. (1997, 1998, 1999a,b) for Fourier methods, de Barros et al. (2006) for a Laplacian model, Suppes et al. (2009) for congruence between brain and perceptual feature of language, and Wong et al. (2006) for perceptron models with regularization and independent component analysis.

The oscillator computations developed in this paper provide a schematic model of psychological processes successfully described behaviorally using stimulus-response theory. The coupled neural phase oscillators used offer a physical mechanism to explain schematically how conditioning works in the brain. But many important physical details of such processes remain to be clarified. The oscillator-simulations do suggest many physically and biologically relevant measurements that are not part of stimulus-response theory. For example, although we used the simplifying assumption that a response occurs at a time Δt_r after the onset of the stimulus, a more detailed model should derive a response-time distribution variance, with mean and variance at least being derived from biological assumptions about various physical processes, such as firing thresholds being reached due to oscillator synchronization. Another feature that could be further explored is the interference between oscillators. As we saw in Section 4, neural oscillators may interfere in ways similar to two electrical oscillators or two wave sources. This interference may lead to predictions distinct from those of classical SR theory, when modeling complex processes. Such predictions could, perhaps, be closer to behavioral models suggested by very different approaches (see (Busemeyer et al., 2006; Bruza et al., 2009) for possible alternatives).

Finally, we emphasize that neural oscillators may produce, in principle, measurable electrophysiological signals. Prior to having such measurements available as psychology and system neuroscience draw closer together, it is desirable that specific, even if only schematic, physical mechanisms be proposed to provide conceptually plausible physical realizations of fundamental psychological processes. The most important idea tested here is that the main physical mechanism in stimulus-response learning

is phase-locking, a concept widely used in physics, but not in psychology, or, even as yet, not much in system neuroscience.

Appendix A. Properties of the Oscillator Model

In this appendix we derive many important properties of the oscillator model. In Section Appendix A.1, we show that the convergence values for the reinforced couplings lead to some fixed points for equations (24)–(26) that correspond to the desired phase differences. Section Appendix A.2 examines the different fixed points, and verifies that the couplings converge to couplings such that the only stable fixed points are those corresponding to the reinforced phase difference $\delta\varphi$. Section Appendix A.3 extends the results of Section Appendix A.2 to the case of different coupling strengths, and establishes a more general condition for the stability of the fixed point corresponding to $\delta\varphi$ based on the relative signs of the couplings. This result is relevant, as the learning equations do not guarantee the exact values of couplings, but they can guarantee, when learning is effective, that couplings do satisfy the conditions presented in Section Appendix A.3. In Section Appendix A.4 we analyze the relationship between coupling strength and the convergence time of equations (24)–(26) toward a fixed point. Section Appendix A.5 investigates the behavior of the oscillators during reinforcement. Finally, in Section Appendix A.6 we show how some of the model parameters relate to the effectiveness of reinforcement θ , deriving equation (47).

Appendix A.1. Fixed points for coding phase relations

Here we derive the asymptotic couplings for the reinforcement angles coding the phase relation $\delta\varphi$ detailed in Section 4, and then show that such couplings lead to a set of differential equations with fixed points that are stable around solutions corresponding to the desired phase differences (18). First, let us start with the reinforcement schedule set such that $\varphi_s = \omega_e t$, $\varphi_{r_1} = \omega_e t + \delta\varphi$, and $\varphi_{r_2} = \omega_e t + \delta\varphi - \pi$. From (28)–(30) we obtain the following fixed points for excitatory connections, which work as an attractor for the asymptotic behavior (for more details, see Appendix A.5).

$$k_{s,r_1}^E = \alpha \cos(\delta\varphi), \quad (\text{Appendix A.1})$$

$$k_{s,r_2}^E = -\alpha \cos(\delta\varphi), \quad (\text{Appendix A.2})$$

$$k_{r_1,r_2}^E = -\alpha, \quad (\text{Appendix A.3})$$

$$k_{r_1,s}^E = \alpha \cos(\delta\varphi), \quad (\text{Appendix A.4})$$

$$k_{r_2,s}^E = -\alpha \cos(\delta\varphi), \quad (\text{Appendix A.5})$$

$$k_{r_2,r_1}^E = -\alpha. \quad (\text{Appendix A.6})$$

Similarly, for inhibitory connections we have.

$$k_{s,r_1}^I = -\alpha \sin(\delta\varphi), \quad (\text{Appendix A.7})$$

$$k_{s,r_2}^I = \alpha \sin(\delta\varphi), \quad (\text{Appendix A.8})$$

$$k_{r_1,r_2}^I = 0, \quad (\text{Appendix A.9})$$

$$k_{r_1,s}^I = \alpha \sin(\delta\varphi), \quad (\text{Appendix A.10})$$

$$k_{r_2,s}^I = -\alpha \sin(\delta\varphi), \quad (\text{Appendix A.11})$$

$$k_{r_2,r_1}^I = 0. \quad (\text{Appendix A.12})$$

Assuming that a sufficient time interval elapsed such that the coupling coefficients converged to (Appendix A.1)–(Appendix A.12), Kuramoto’s equations become

$$\begin{aligned}
\frac{d\varphi_s}{dt} &= \omega_0 - \alpha \cos(\delta\varphi) \sin(\varphi_s - \varphi_{r_1}) \\
&\quad + \alpha \cos(\delta\varphi) \sin(\varphi_s - \varphi_{r_2}) \\
&\quad + \alpha \sin(\delta\varphi) \cos(\varphi_s - \varphi_{r_1}) \\
&\quad - \alpha \sin(\delta\varphi) \cos(\varphi_s - \varphi_{r_2}), \\
\frac{d\varphi_{r_1}}{dt} &= \omega_0 - \alpha \cos(\delta\varphi) \sin(\varphi_{r_1} - \varphi_s) \\
&\quad + \alpha \sin(\varphi_{r_1} - \varphi_{r_2}) \\
&\quad - \alpha \sin(\delta\varphi) \cos(\varphi_{r_1} - \varphi_s), \\
\frac{d\varphi_{r_2}}{dt} &= \omega_0 + \alpha \cos(\delta\varphi) \sin(\varphi_{r_2} - \varphi_s) \\
&\quad + \alpha \sin(\varphi_{r_2} - \varphi_{r_1}) \\
&\quad + \alpha \sin(\delta\varphi) \cos(\varphi_{r_2} - \varphi_s).
\end{aligned}$$

Regrouping the terms with the same phase oscillators, we have

$$\begin{aligned}
\frac{d\varphi_s}{dt} &= \omega_0 - \alpha \sin(\varphi_s - \varphi_{r_1} + \delta\varphi) \\
&\quad + \alpha \sin(\varphi_s - \varphi_{r_2} + \delta\varphi), \\
\frac{d\varphi_{r_1}}{dt} &= \omega_0 - \alpha \sin(\varphi_{r_1} - \varphi_s - \delta\varphi) \\
&\quad + \alpha \sin(\varphi_{r_1} - \varphi_{r_2}), \\
\frac{d\varphi_{r_2}}{dt} &= \omega_0 + \alpha \sin(\varphi_{r_2} - \varphi_s - \delta\varphi) \\
&\quad + \alpha \sin(\varphi_{r_2} - \varphi_{r_1}),
\end{aligned}$$

or

$$\begin{aligned}
\frac{d\varphi_s}{dt} &= \omega_0 - \alpha \sin(\varphi_s - \varphi_{r_1} + \delta\varphi) \\
&\quad - \alpha \sin(\varphi_s - \varphi_{r_2} + \delta\varphi - \pi), \tag{Appendix A.13}
\end{aligned}$$

$$\begin{aligned}
\frac{d\varphi_{r_1}}{dt} &= \omega_0 - \alpha \sin(\varphi_{r_1} - \varphi_s - \delta\varphi) \\
&\quad - \alpha \sin(\varphi_{r_1} - \varphi_{r_2} - \pi), \tag{Appendix A.14}
\end{aligned}$$

$$\begin{aligned}
\frac{d\varphi_{r_2}}{dt} &= \omega_0 - \alpha \sin(\varphi_{r_2} - \varphi_s - \delta\varphi + \pi) \\
&\quad - \alpha \sin(\varphi_{r_2} - \varphi_{r_1} + \pi). \tag{Appendix A.15}
\end{aligned}$$

It is straightforward to verify that equations (Appendix A.13)–(Appendix A.15) have the desired phase relations as fixed points. In the next section, we will show that not only are those fixed points stable, but that they are the only stable points modulo a 2π transformation (which in our case is not relevant).

Appendix A.2. Stability of Fixed Points

In Appendix A.1, we showed that a specific choice of couplings in the Kuramoto equations leads to a specific phase relation between oscillators. Here we derive the stability conditions. We assume that the couplings are such as required by phase differences $\varphi_s = \varphi_{r_1} - \delta\varphi$ and $\varphi_{r_1} = \varphi_{r_2} + \pi$, as coded in couplings (Appendix A.1)–(Appendix A.12). To simplify our approach, we start with equations

(Appendix A.13)–(Appendix A.15) and make the following change of variables:

$$\begin{aligned}\phi_s &= \varphi_s + \delta\varphi, \\ \phi_1 &= \varphi_{r_1}, \\ \phi_2 &= \varphi_{r_2} + \pi.\end{aligned}$$

Equations (Appendix A.13)–(Appendix A.15) then become

$$\begin{aligned}\frac{d\phi_s}{dt} &= \omega_0 - \alpha \sin(\phi_s - \phi_1) \\ &\quad - \alpha \sin(\phi_s - \phi_2),\end{aligned}\tag{Appendix A.16}$$

$$\begin{aligned}\frac{d\phi_1}{dt} &= \omega_0 - \alpha \sin(\phi_1 - \phi_s) \\ &\quad - \alpha \sin(\phi_1 - \phi_2),\end{aligned}\tag{Appendix A.17}$$

$$\begin{aligned}\frac{d\phi_2}{dt} &= \omega_0 - \alpha \sin(\phi_2 - \phi_s) \\ &\quad - \alpha \sin(\phi_2 - \phi_1).\end{aligned}\tag{Appendix A.18}$$

This change of variables allow us to re-write the dynamical equations without any references to the specific phase differences, and therefore we can obtain general results for any phase differences consistent with the desired relations for conditioning. Additionally, since we are mainly interested in phase differences, we make yet another change of variables, further simplifying our equations, by defining

$$\begin{aligned}\phi_{1s} &= \phi_1 - \phi_s, \\ \phi_{2s} &= \phi_2 - \phi_s.\end{aligned}$$

Substituting in (Appendix A.16)–(Appendix A.18), we reduce the system to the following pair of coupled differential equations.

$$\begin{aligned}\frac{d\phi_{1s}}{dt} &= -2\alpha \sin(\phi_{1s}) - \alpha \sin(\phi_{2s}) \\ &\quad - \alpha \sin(\phi_{1s} - \phi_{2s}),\end{aligned}\tag{Appendix A.19}$$

$$\begin{aligned}\frac{d\phi_{2s}}{dt} &= -\alpha \sin(\phi_{1s}) - 2\alpha \sin(\phi_{2s}) \\ &\quad + \alpha \sin(\phi_{1s} - \phi_{2s}).\end{aligned}\tag{Appendix A.20}$$

Because we are interested in general properties of stability, and we want to understand what conditions lead to the stable desired fixed points, it is convenient to not restrict our couplings to the ones imposed by a specific phase relation. Instead, we rewrite the above differential equations in terms of couplings that are not necessarily all the same, i.e.,

$$\begin{aligned}\frac{d\phi_{1s}}{dt} &= -2k_{s,r_1} \sin(\phi_{1s}) - k_{s,r_2} \sin(\phi_{2s}) \\ &\quad - k_{r_1,r_2} \sin(\phi_{1s} - \phi_{2s}),\end{aligned}\tag{Appendix A.21}$$

$$\begin{aligned}\frac{d\phi_{2s}}{dt} &= -k_{s,r_1} \sin(\phi_{1s}) - 2k_{s,r_2} \sin(\phi_{2s}) \\ &\quad + k_{r_1,r_2} \sin(\phi_{1s} - \phi_{2s}).\end{aligned}\tag{Appendix A.22}$$

The only constraint we will make later on in our analysis is that such couplings need to have the same absolute value, a requirement consistent with asymptotic behavior of the learning equations (see Appendix A.5). Right now, the question we want to answer is the following. Are there stable solutions to (Appendix A.21) and (Appendix A.22)? If so, how do they depend on the couplings?

To answer the above questions, we should first compute whether there are any fixed points for differential equations (Appendix A.21) and (Appendix A.22). Since a fixed point is a point where the system remains if initially placed in it, they are characterized by having both time derivatives of ϕ_{1j} and ϕ_{2j} equal to zero. Thus, the fixed points are given by

$$-2k_{s,r_1} \sin(\phi_{1s}) - k_{s,r_2} \sin(\phi_{2s}) \quad (\text{Appendix A.23})$$

$$-k_{r_1,r_2} \sin(\phi_{1s} - \phi_{2s}) = 0,$$

$$-k_{s,r_1} \sin(\phi_{1s}) - 2k_{s,r_2} \sin(\phi_{2s}) \quad (\text{Appendix A.24})$$

$$+k_{r_1,r_2} \sin(\phi_{1s} - \phi_{2s}) = 0.$$

Because of the periodicity of the sine function, there are infinitely many fixed points. Since we are interested in phases, we do not need to examine all points, but it suffices to focus on the region determined by $0 \leq \phi_{1s} < 2\pi$ and $0 \leq \phi_{2s} < 2\pi$. The trivial fixed points, corresponding to each sine function in (Appendix A.23) and (Appendix A.24) being zero, are $(0, 0)$, $(\pi, 0)$, $(0, \pi)$, and (π, π) . The other solutions depend on the values of the coupling constants. To simplify our analysis, let us consider the case where all couplings have the same magnitude, i.e. $|k_{s,r_1}| = |k_{r_1,r_2}| = |k_{s,r_2}|$. Since the relative coupling strengths are relevant for matters of stability, let us consider the following scenarios: $k \equiv k_{s,r_1} = k_{s,r_2} = k_{r_1,r_2}$, $k \equiv -k_{s,r_1} = k_{s,r_2} = k_{r_1,r_2}$, $k \equiv k_{s,r_1} = -k_{s,r_2} = k_{r_1,r_2}$, and $k \equiv k_{s,r_1} = k_{s,r_2} = -k_{r_1,r_2}$. Other cases, like $-k_{s,r_1} = -k_{s,r_2} = k_{r_1,r_2}$, are contained in those, since k can be either positive or negative. Let us examine each case separately.

Appendix A.2.1. $k \equiv k_{s,r_1} = k_{s,r_2} = k_{r_1,r_2}$

For this case, in addition to $\{(0, 0), (0, \pi), (\pi, 0), (\pi, \pi)\}$, we have $(\frac{2}{3}\pi, -\frac{2}{3}\pi)$ and $(-\frac{2}{3}\pi, \frac{2}{3}\pi)$ as fixed points. Let us start with $\{(0, 0), (0, \pi), (\pi, 0), (\pi, \pi)\}$. In order to analyze their local stability, we linearize Kuramoto's equations (Appendix A.21) and (Appendix A.22) around $\{(0, 0), (0, \pi), (\pi, 0), (\pi, \pi)\}$. To linearize the equations, first we substitute ϕ_{1s} and ϕ_{2s} by $a + \epsilon_1$ and $b + \epsilon_2$, where a and b are the coordinates of the fixed points. Then we make a linear approximation for the sine function for values close to the fixed point, i.e. for ϵ_1 and ϵ_2 being small. Below we show the linearized equations for different fixed points (a, b) .

For example, for $(0, \pi)$ we define $\phi_{1s} = \epsilon_1$ and $\phi_{2s} = \pi + \epsilon_2$. Then (Appendix A.21) and (Appendix A.22) become

$$\frac{d\epsilon_1}{dt} = -2k \sin(\epsilon_1) - k \sin(\pi + \epsilon_2) \quad (\text{Appendix A.25})$$

$$-k \sin(\epsilon_1 - \epsilon_2 - \pi),$$

$$\frac{d\epsilon_2}{dt} = -k \sin(\epsilon_1) - 2k \sin(\pi + \epsilon_2) \quad (\text{Appendix A.26})$$

$$+k \sin(\epsilon_1 - \epsilon_2 - \pi).$$

Because close to the fixed points $\epsilon_1 \ll 1$ and $\epsilon_2 \ll 1$, we make the approximation that $\sin(\epsilon_1) \approx \epsilon_1$ and $\sin(\epsilon_2) \approx \epsilon_2$, and (Appendix A.25) and (Appendix A.26) can be written as

$$\frac{d\epsilon_1}{dt} = -2k\epsilon_1 + k\epsilon_2 + k(\epsilon_1 - \epsilon_2), \quad (\text{Appendix A.27})$$

$$\frac{d\epsilon_2}{dt} = -k\epsilon_1 + 2k\epsilon_2 - k(\epsilon_1 - \epsilon_2), \quad (\text{Appendix A.28})$$

or

$$\frac{d\epsilon_1}{dt} = -k\epsilon_1, \quad (\text{Appendix A.29})$$

$$\frac{d\epsilon_2}{dt} = -2k\epsilon_1 + 3k\epsilon_2. \quad (\text{Appendix A.30})$$

The eigenvalues for the linearized (Appendix A.29) and (Appendix A.30) are $-k$ and $3k$. A fixed point is Liapunov stable if its eigenvalues are negative (Guckenheimer and Holmes, 1983). Therefore, for $k \equiv k_{s,r_1} = k_{s,r_2} = k_{r_1,r_2}$, the fixed point $(0, \pi)$ cannot be stable.

We perform the same computations for the other fixed points. The linearized equations are

$$\frac{d\epsilon_1}{dt} = -3k\epsilon_1, \quad (\text{Appendix A.31})$$

$$\frac{d\epsilon_2}{dt} = -3k\epsilon_2, \quad (\text{Appendix A.32})$$

for $(0, 0)$,

$$\frac{d\epsilon_1}{dt} = -k\epsilon_1, \quad (\text{Appendix A.33})$$

$$\frac{d\epsilon_2}{dt} = -2k\epsilon_1 + 3k\epsilon_2, \quad (\text{Appendix A.34})$$

once again, for $(0, \pi)$,

$$\frac{d\epsilon_1}{dt} = 3k\epsilon_1 - 2k\epsilon_2, \quad (\text{Appendix A.35})$$

$$\frac{d\epsilon_2}{dt} = -k\epsilon_2, \quad (\text{Appendix A.36})$$

for $(\pi, 0)$, and

$$\frac{d\epsilon_1}{dt} = k\epsilon_1 + 2k\epsilon_2, \quad (\text{Appendix A.37})$$

$$\frac{d\epsilon_2}{dt} = 2k\epsilon_1 + k\epsilon_2, \quad (\text{Appendix A.38})$$

for (π, π) . Only (Appendix A.31) and (Appendix A.32) have negative eigenvalues, when $k > 0$, thus corresponding to stable fixed points.

Now let us examine fixed points $(\frac{2}{3}\pi, -\frac{2}{3}\pi)$ and $(-\frac{2}{3}\pi, \frac{2}{3}\pi)$. Substituting $\phi_{1s} = \pm\frac{2}{3}\pi + \epsilon_1(t)$ and $\phi_{2s} = \mp\frac{2}{3}\pi + \epsilon_2(t)$ in (Appendix A.21) and (Appendix A.22), we have

$$\begin{aligned} \frac{1}{k} \frac{d\epsilon_1}{dt} &= -2 \sin\left(\pm\frac{2}{3}\pi + \epsilon_1\right) - \sin\left(\mp\frac{2}{3}\pi + \epsilon_2\right) \\ &\quad - \sin\left(\pm\frac{2}{3}\pi + \epsilon_1(t) \pm \frac{2}{3}\pi - \epsilon_2\right), \end{aligned} \quad (\text{Appendix A.39})$$

$$\begin{aligned} \frac{1}{k} \frac{d\epsilon_2}{dt} &= -\sin\left(\pm\frac{2}{3}\pi + \epsilon_1\right) - 2 \sin\left(\mp\frac{2}{3}\pi + \epsilon_2\right) \\ &\quad + \sin\left(\pm\frac{2}{3}\pi + \epsilon_1(t) \pm \frac{2}{3}\pi - \epsilon_2\right). \end{aligned} \quad (\text{Appendix A.40})$$

Using the linear approximation for $\epsilon_1 \ll 1$ and $\epsilon_2 \ll 1$ we get

$$\begin{aligned} \frac{1}{k} \frac{d\epsilon_1}{dt} &= \mp 2 \sin\left(\frac{2}{3}\pi\right) - 2 \cos\left(\frac{2}{3}\pi\right) \epsilon_1 \\ &\quad \pm \sin\left(\frac{2}{3}\pi\right) - \cos\left(\frac{2}{3}\pi\right) \epsilon_2 \\ &\quad \mp \sin\left(\frac{4}{3}\pi\right) \\ &\quad - \cos\left(\frac{4}{3}\pi\right) (\epsilon_1 - \epsilon_2), \end{aligned} \tag{Appendix A.41}$$

$$\begin{aligned} \frac{1}{k} \frac{d\epsilon_2}{dt} &= \mp \sin\left(\frac{2}{3}\pi\right) - \cos\left(\frac{2}{3}\pi\right) \epsilon_1 \\ &\quad \pm 2 \sin\left(\frac{2}{3}\pi\right) - 2 \cos\left(\frac{2}{3}\pi\right) \epsilon_2 \\ &\quad \pm \sin\left(\frac{4}{3}\pi\right) \\ &\quad + \cos\left(\frac{4}{3}\pi\right) (\epsilon_1 - \epsilon_2). \end{aligned} \tag{Appendix A.42}$$

or

$$\frac{1}{k} \frac{d\epsilon_1}{dt} = \frac{3}{2} \epsilon_1, \tag{Appendix A.43}$$

$$\frac{1}{k} \frac{d\epsilon_2}{dt} = \frac{3}{2} \epsilon_2. \tag{Appendix A.44}$$

This point is stable if $k < 0$. Thus, for $k \equiv k_{s,r_1} = k_{s,r_2} = k_{r_1,r_2}$, there are three stable fixed points: $(0, 0)$, $(\frac{2}{3}\pi, -\frac{2}{3}\pi)$, and $(-\frac{2}{3}\pi, \frac{2}{3}\pi)$. However, if $k > 0$ the only fixed point that is stable is $(0, 0)$, corresponding to the situation when all oscillators are exactly in phase.

Appendix A.2.2. $k \equiv -k_{s,r_1} = k_{s,r_2} = k_{r_1,r_2}$

Now the fixed points are $(0, 0)$, $(0, \pi)$, $(\pi, 0)$, (π, π) , $(\frac{2}{3}\pi, \frac{1}{3}\pi)$, and $(-\frac{2}{3}\pi, -\frac{1}{3}\pi)$. The linearized equations are

$$\frac{d\epsilon_1}{dt} = k\epsilon_1, \tag{Appendix A.45}$$

$$\frac{d\epsilon_2}{dt} = 2k\epsilon_1 - 3k\epsilon_2, \tag{Appendix A.46}$$

for $(0, 0)$,

$$\frac{d\epsilon_1}{dt} = 3k\epsilon_1, \tag{Appendix A.47}$$

$$\frac{d\epsilon_2}{dt} = 3k\epsilon_2, \tag{Appendix A.48}$$

for $(0, \pi)$,

$$\frac{d\epsilon_1}{dt} = -k\epsilon_1 - 2k\epsilon_2, \tag{Appendix A.49}$$

$$\frac{d\epsilon_2}{dt} = -2k\epsilon_1 - k\epsilon_2, \tag{Appendix A.50}$$

for $(\pi, 0)$, and

$$\frac{d\epsilon_1}{dt} = -3k\epsilon_1 + 2k\epsilon_2, \quad (\text{Appendix A.51})$$

$$\frac{d\epsilon_2}{dt} = k\epsilon_2, \quad (\text{Appendix A.52})$$

for (π, π) . Only (Appendix A.47) and (Appendix A.48) correspond to fixed points that can be stable, if $k < 0$, as there are no other choices of k that would allow the other points to be stable.

For fixed points $(\frac{2}{3}\pi, \frac{1}{3}\pi)$ and $(-\frac{2}{3}\pi, -\frac{1}{3}\pi)$, we substitute $\phi_{1s} = \pm\frac{2}{3}\pi + \epsilon_1(t)$ and $\phi_{2s} = \pm\frac{1}{3}\pi + \epsilon_2(t)$ in (Appendix A.21) and (Appendix A.22), and we have

$$\begin{aligned} \frac{d\epsilon_1}{dt} &= 2k \sin\left(\pm\frac{2}{3}\pi + \epsilon_1\right) - k \sin\left(\pm\frac{1}{3}\pi + \epsilon_2\right) \\ &\quad - k \sin\left(\pm\frac{2}{3}\pi \mp \frac{1}{3}\pi + \epsilon_1 - \epsilon_2\right), \end{aligned} \quad (\text{Appendix A.53})$$

$$\begin{aligned} \frac{d\epsilon_2}{dt} &= k \sin\left(\pm\frac{2}{3}\pi + \epsilon_1\right) - 2k \sin\left(\pm\frac{1}{3}\pi + \epsilon_2\right) \\ &\quad + k \sin\left(\pm\frac{2}{3}\pi \mp \frac{1}{3}\pi + \epsilon_1 - \epsilon_2\right). \end{aligned} \quad (\text{Appendix A.54})$$

Using the linear approximation for $\epsilon_1 \ll 1$ and $\epsilon_2 \ll 1$ we get

$$\frac{1}{k} \frac{d\epsilon_1}{dt} = -\frac{3}{2}\epsilon_1, \quad (\text{Appendix A.55})$$

$$\frac{1}{k} \frac{d\epsilon_2}{dt} = -\frac{3}{2}\epsilon_2. \quad (\text{Appendix A.56})$$

Points $(\frac{2}{3}\pi, \frac{1}{3}\pi)$ and $(-\frac{2}{3}\pi, -\frac{1}{3}\pi)$ are stable if $k > 0$. Thus, for $k \equiv -k_{s,r_1} = k_{s,r_2} = k_{r_1,r_2}$, there are three relevant stable fixed points: $(0, \pi)$, $(\frac{2}{3}\pi, \frac{1}{3}\pi)$ and $(-\frac{2}{3}\pi, -\frac{1}{3}\pi)$. However, if $k < 0$ the only fixed point that is stable is $(0, \pi)$, corresponding to the situation when the oscillators s and r_1 are in phase and s and r_2 are off phase by π .

Appendix A.2.3. $k \equiv k_{s,r_1} = -k_{s,r_2} = k_{r_1,r_2}$

For the points $\{(0, 0), (0, \pi), (\pi, 0), (\pi, \pi)\}$ the linearized form of (Appendix A.55) and (Appendix A.56) around the stability points are

$$\frac{d\epsilon_1}{dt} = -3k\epsilon_1 + 2k\epsilon_2, \quad (\text{Appendix A.57})$$

$$\frac{d\epsilon_2}{dt} = k\epsilon_2, \quad (\text{Appendix A.58})$$

for $(0, 0)$,

$$\frac{d\epsilon_1}{dt} = -k\epsilon_1 - 2k\epsilon_2, \quad (\text{Appendix A.59})$$

$$\frac{d\epsilon_2}{dt} = -2k\epsilon_1 - k\epsilon_2, \quad (\text{Appendix A.60})$$

for $(0, \pi)$,

$$\frac{d\epsilon_1}{dt} = 3k\epsilon_1, \quad (\text{Appendix A.61})$$

$$\frac{d\epsilon_2}{dt} = 3k\epsilon_2, \quad (\text{Appendix A.62})$$

for $(\pi, 0)$, and

$$\frac{d\epsilon_1}{dt} = k\epsilon_1, \quad (\text{Appendix A.63})$$

$$\frac{d\epsilon_2}{dt} = 2k\epsilon_1 - 3k\epsilon_2, \quad (\text{Appendix A.64})$$

for (π, π) . Only (Appendix A.61) and (Appendix A.62) correspond to fixed points that can be stable, if we choose $k < 0$. There are no choices of k that would allow the other points to be stable.

The other stable points are $(\frac{1}{3}\pi, \frac{2}{3}\pi)$ and $(-\frac{1}{3}\pi, -\frac{2}{3}\pi)$. The linearized (Appendix A.21) and (Appendix A.22) become

$$\begin{aligned} \frac{1}{k} \frac{d\epsilon_1}{dt} &= -2 \sin\left(\pm \frac{1}{3}\pi + \epsilon_1\right) + \sin\left(\pm \frac{2}{3}\pi + \epsilon_2\right) \\ &\quad - \sin\left(\pm \frac{1}{3}\pi + \epsilon_1 \mp \frac{2}{3}\pi - \epsilon_2\right), \end{aligned} \quad (\text{Appendix A.65})$$

$$\begin{aligned} \frac{1}{k} \frac{d\epsilon_2}{dt} &= -\sin\left(\pm \frac{1}{3}\pi + \epsilon_1\right) + 2 \sin\left(\pm \frac{2}{3}\pi + \epsilon_2\right) \\ &\quad + \sin\left(\pm \frac{1}{3}\pi + \epsilon_1 \mp \frac{2}{3}\pi - \epsilon_2\right). \end{aligned} \quad (\text{Appendix A.66})$$

Using the linear approximation for $\epsilon_1 \ll 1$ and $\epsilon_2 \ll 1$ we get

$$\begin{aligned} \frac{1}{k} \frac{d\epsilon_1}{dt} &= -\frac{3}{2}\epsilon_1, \\ \frac{1}{k} \frac{d\epsilon_2}{dt} &= -\frac{3}{2}\epsilon_2. \end{aligned}$$

This point is stable if $k > 0$. Thus, for $k \equiv k_{s,r_1} = -k_{s,r_2} = k_{r_1,r_2}$ there are three relevant stable fixed points: $(\pi, 0)$, $(\frac{1}{3}\pi, \frac{2}{3}\pi)$, and $(-\frac{1}{3}\pi, -\frac{2}{3}\pi)$, but if $k < 0$ only the point $(\pi, 0)$ is stable, corresponding to oscillator r_2 in phase with oscillator s , and r_1 off phase with s .

Appendix A.2.4. $k \equiv k_{s,r_1} = k_{s,r_2} = -k_{r_1,r_2}$

For the points $\{(0, 0), (0, \pi), (\pi, 0), (\pi, \pi)\}$, linearizing (Appendix A.55) and (Appendix A.56) gives us

$$\frac{d\epsilon_1}{dt} = -3k\epsilon_1, \quad (\text{Appendix A.67})$$

$$\frac{d\epsilon_2}{dt} = k\epsilon_2, \quad (\text{Appendix A.68})$$

for $(0, 0)$,

$$\frac{d\epsilon_1}{dt} = -3k\epsilon_1 + 2k\epsilon_2, \quad (\text{Appendix A.69})$$

$$\frac{d\epsilon_2}{dt} = k\epsilon_2, \quad (\text{Appendix A.70})$$

for $(0, \pi)$,

$$\frac{d\epsilon_1}{dt} = k\epsilon_1, \quad (\text{Appendix A.71})$$

$$\frac{d\epsilon_2}{dt} = 2k\epsilon_1 - 3k\epsilon_2, \quad (\text{Appendix A.72})$$

	$k_{s,r_1} > 0$	$k_{s,r_1} < 0$
$k_{s,r_1} = k_{s,r_2} = k_{r_1,r_2}$	$(0, 0)$	$(\frac{2}{3}\pi, -\frac{2}{3}\pi)$ $(-\frac{2}{3}\pi, \frac{2}{3}\pi)$
$-k_{s,r_1} = k_{s,r_2} = k_{r_1,r_2}$	$(\frac{2}{3}\pi, \frac{1}{3}\pi)$ $(-\frac{2}{3}\pi, -\frac{1}{3}\pi)$	$(0, \pi)$
$k_{s,r_1} = -k_{s,r_2} = k_{r_1,r_2}$	$(\frac{1}{3}\pi, \frac{2}{3}\pi)$ $(-\frac{1}{3}\pi, -\frac{2}{3}\pi)$	$(\pi, 0)$
$k_{s,r_1} = k_{s,r_2} = -k_{r_1,r_2}$	$(-\frac{1}{3}\pi, \frac{1}{3}\pi)$ $(\frac{1}{3}\pi, -\frac{1}{3}\pi)$	(π, π)

Table A.4: Stable fixed points for $|k_{s,r_1}| = |k_{s,r_2}| = |k_{r_1,r_2}|$. Since the absolute values of the coupling strengths are all the same, which fixed points are stable is determined by the relative signs of the couplings.

for $(\pi, 0)$, and

$$\frac{d\epsilon_1}{dt} = 3k\epsilon_1, \quad (\text{Appendix A.73})$$

$$\frac{d\epsilon_2}{dt} = 3k\epsilon_2, \quad (\text{Appendix A.74})$$

for (π, π) . Once again, only (Appendix A.73) and (Appendix A.74) correspond to fixed points that can be stable, if we choose $k < 0$.

The other fixed points are $(-\frac{1}{3}\pi, \frac{1}{3}\pi)$ and $(\frac{1}{3}\pi, -\frac{1}{3}\pi)$. Substituting $\phi_{1s} = \mp\frac{1}{3}\pi + \epsilon_1(t)$ and $\phi_{2s} = \pm\frac{1}{3}\pi + \epsilon_2(t)$ in (Appendix A.21) and (Appendix A.22), after a linear approximation for $\epsilon_1 \ll 1$ and $\epsilon_2 \ll 1$, we obtain

$$\frac{1}{k} \frac{d\epsilon_1}{dt} = -\frac{3}{2}\epsilon_1, \quad (\text{Appendix A.75})$$

$$\frac{1}{k} \frac{d\epsilon_2}{dt} = -\frac{3}{2}\epsilon_2. \quad (\text{Appendix A.76})$$

This point is stable if $k > 0$. For $k \equiv k_{s,r_1} = k_{s,r_2} = -k_{r_1,r_2}$ there are three relevant stable fixed points: (π, π) , $(\frac{2}{3}\pi, -\frac{2}{3}\pi)$, and $(-\frac{2}{3}\pi, \frac{2}{3}\pi)$.⁴ However, if $k < 0$ the only fixed point that is stable is (π, π) , corresponding to the situation when both oscillators r_1 and r_2 are off phase with respect to oscillator s by π .

The results of Sections Appendix A.2.1–Appendix A.2.4 are summarized in Table A.4. If $k_{s,r_1} < 0$, the relative signs of the other coupling constants determine unique stability points, corresponding to oscillator r_1 in phase with oscillator s and r_2 off phase by π (row 2), r_2 in phase and r_1 off phase by π (row 3), and both r_1 and r_2 off phase by π (row 4). The only possibility for all oscillators r_1 , r_2 , and s to be in phase is when all couplings are positive.

Appendix A.3. General sufficient criteria

In the section above, we showed how the fixed points behaved for couplings with the same strength but different signs. But, since the learning equations (28)-(42) and the initial conditions cannot guarantee couplings with the same strength, we need to show that a fixed point is stable under even if the couplings have different strengths. Here, we show a more general condition for stability. Let us

⁴In fact we have, as discussed above, an infinite number of stable fixed points. But since we are only interested in phase differences, and the fixed points other than $(\frac{2}{3}\pi, -\frac{2}{3}\pi)$ and $(-\frac{2}{3}\pi, \frac{2}{3}\pi)$ are periodic, with periodicity 2π , we omit them from our discussion.

take, for instance, the point $(0, \pi)$. Close to this point, Equations (Appendix A.21)-(Appendix A.22), after linearization, become

$$\begin{aligned} \frac{d\epsilon_1}{dt} &= -2k_{s,r_1}\epsilon_1 + k_{s,r_2}\epsilon_2 \\ &\quad + k_{r_1,r_2}(\epsilon_1 - \epsilon_2), \end{aligned} \quad (\text{Appendix A.77})$$

$$\begin{aligned} \frac{d\epsilon_2}{dt} &= -k_{s,r_1}\epsilon_1 + 2k_{s,r_2}\epsilon_2 \\ &\quad - k_{r_1,r_2}(\epsilon_1 - \epsilon_2). \end{aligned} \quad (\text{Appendix A.78})$$

Equations (Appendix A.77) and (Appendix A.78) have eigenvalues

$$\lambda_1 = -k_{s,r_1} + k_{r_1,r_2} + k_{s,r_2} - \sqrt{D}, \quad (\text{Appendix A.79})$$

and

$$\lambda_2 = -k_{s,r_1} + k_{r_1,r_2} + k_{s,r_2} + \sqrt{D}, \quad (\text{Appendix A.80})$$

where

$$\begin{aligned} D &= k_{s,r_1}^2 + k_{s,r_1}k_{r_1,r_2} + k_{r_1,r_2}^2 \\ &\quad + k_{s,r_1}k_{s,r_2} - k_{s,r_2}k_{r_1,r_2} + k_{s,r_2}^2. \end{aligned}$$

The stability point $(0, \pi)$ is stable if the eigenvalues λ_1 and λ_2 are negative. Since $\lambda_2 < 0$ implies $\lambda_1 < 0$, we focus on Equation (Appendix A.80). As long as the couplings are real, we can show that $D \geq 0$. Thus, the requirement that in (Appendix A.80), λ_2 is negative is equivalent to

$$\begin{aligned} (k_{s,r_1} - k_{s,r_2} - k_{r_1,r_2})^2 &> k_{s,r_1}^2 + k_{s,r_1}k_{r_1,r_2} \\ &\quad + k_{r_1,r_2}^2 + k_{s,r_1}k_{s,r_2} \\ &\quad - k_{s,r_2}k_{r_1,r_2} + k_{s,r_2}^2, \end{aligned}$$

which simplifies to

$$k_{s,r_2}k_{r_1,r_2} > k_{s,r_1}k_{r_1,r_2} + k_{s,r_1}k_{s,r_2}. \quad (\text{Appendix A.81})$$

Equation (Appendix A.81) is a sufficient condition for the stability of the point $(0, \pi)$. Using the same technique, similar conditions can be obtained for different fixed points.

Appendix A.4. Time of convergence

As we showed in Equation (Appendix A.81), what determines whether a point is stable or not are the relations between the different oscillator couplings. For example, Equation (Appendix A.81) could be satisfied for a set of k 's that are very small, such as $k_{s,r_2} = .01$, $k_{r_1,r_2} = .01$, and $k_{s,r_1} = .0001$. However, since we are interested in biologically relevant models, showing that the equations of motion asymptotically converges to a fixed point for these values is not sufficient. We need to show that such convergence can happen within a reasonably short amount of time Δt_r , such that responses associated to the fixed points are correctly selected, after effective reinforcement. In this section we will estimate the values of the couplings such that the we should expect fast convergence. To do this, let us focus on the case of $k_{s,r_1} = -k_{s,r_2} = -k_{r_1,r_2} \equiv k$, $k > 0$, discussed in Appendix A.2.2. In this case, the Kuramoto equations are

$$\begin{aligned} \frac{d\phi_{1s}}{dt} &= -2k \sin(\phi_{1s}) + k \sin(\phi_{2s}) \\ &\quad + k \sin(\phi_{1s} - \phi_{2s}), \end{aligned} \quad (\text{Appendix A.82})$$

$$\begin{aligned} \frac{d\phi_{2s}}{dt} &= -k \sin(\phi_{1s}) + 2k \sin(\phi_{2s}) \\ &\quad - k \sin(\phi_{1s} - \phi_{2s}), \end{aligned} \quad (\text{Appendix A.83})$$

and for $(0, \pi)$ we define $\phi_{1s} = \epsilon_1$ and $\phi_{2s} = \pi + \epsilon_2$. Then (Appendix A.82) and (Appendix A.83) become

$$\frac{d\epsilon_1}{dt} = -3k\epsilon_1, \quad (\text{Appendix A.84})$$

$$\frac{d\epsilon_2}{dt} = -3k\epsilon_2. \quad (\text{Appendix A.85})$$

We emphasize that equations are just an approximation for the system close to the fixed point $(0, \pi)$. However, because of the sine terms in Kuramoto's equation, this is a reasonably good approximation, with an error of the order of $O(\epsilon_1^3, \epsilon_2^3)$. Thus, for points close to $(0, \pi)$, the solutions to (Appendix A.82) and (Appendix A.83) are

$$\phi_{1s}(t) = \phi_{1s}(0) e^{-3kt},$$

and

$$\phi_{2s}(t) = \pi + [\phi_{2s}(0) - \pi] e^{-3kt},$$

where $\phi_{1s}(0)$ and $\phi_{2s}(0)$ are the initial conditions. This is an exponential decay converging to the fixed point, and of course neither of the solutions go, within a finite amount of time, to $(0, \pi)$. However, the constant $\tau = 1/3k$ gives us the mean lifetime of the system, thus giving a measure of how fast the convergence to the fixed point is happening. Thus, if we expect the mean lifetime to be at least of the order of $\Delta t_r = 200$ ms, k needs to be approximately 2 Hz. For practical purposes, if we have $k \gg 2$ Hz, our system should converge most of the time within the expected time Δt_r , a result consistent with our numerical simulations.

Appendix A.5. Synchronization of oscillators during reinforcement

We are interested in knowing the qualitative behavior of the phases when a reinforcement occurs. During reinforcement, the oscillators satisfy equations

$$\begin{aligned} \frac{d\varphi_s}{dt} &= +K_0 \sin(\varphi_s - \omega_e t) \\ &\quad \omega_0 - k_{s,r_1} \sin(\varphi_s - \varphi_{r_1}) \\ &\quad - k_{s,r_2} \sin(\varphi_s - \varphi_{r_2}), \end{aligned} \quad (\text{Appendix A.86})$$

$$\begin{aligned} \frac{d\varphi_{r_1}}{dt} &= K_0 \sin(\varphi_{r_1} - \omega_e t - \pi(1 - \delta_{E_n,1})) \\ &\quad + \omega_0 - k_{s,r_1} \sin(\varphi_{r_1} - \varphi_s) \\ &\quad - k_{r_1,r_2} \sin(\varphi_{r_1} - \varphi_{r_2}), \end{aligned} \quad (\text{Appendix A.87})$$

$$\begin{aligned} \frac{d\varphi_{r_2}}{dt} &= K_0 \sin(\varphi_{r_2} - \omega_e t - \pi(1 - \delta_{E_n,2})) \\ &\quad + \omega_0 - k_{s,r_2} \sin(\varphi_{r_2} - \varphi_s) \\ &\quad - k_{r_1,r_2} \sin(\varphi_{r_2} - \varphi_{r_1}), \end{aligned} \quad (\text{Appendix A.88})$$

$$\frac{dk_{s,r_1}}{dt} = \epsilon(K_0) [\alpha \cos(\varphi_s - \varphi_{r_1}) - k_{s,r_1}], \quad (\text{Appendix A.89})$$

$$\frac{dk_{s,r_2}}{dt} = \epsilon(K_0) [\alpha \cos(\varphi_s - \varphi_{r_2}) - k_{s,r_2}], \quad (\text{Appendix A.90})$$

$$\frac{dk_{r_1,r_2}}{dt} = \epsilon(K_0) [\alpha \cos(\varphi_{r_1} - \varphi_{r_2}) - k_{r_1,r_2}], \quad (\text{Appendix A.91})$$

where E_n is either 1 or 2 depending on which finite response is being reinforced, and $\delta_{i,j}$ is Kronecker's delta, i.e., $\delta_{E_n,2}$ is one if $E_n = 2$ and zero otherwise. We show here that the first three equations lead the oscillators s , r_1 , and r_2 to synchronize and phase lock with reinforcement oscillators e_1 and e_2 if K_0 is sufficiently large. We start with the approximation

$$\dot{\varphi}_s \approx \omega_0 + K_0 \sin(\varphi_s - \omega_e t),$$

for $K_0 \gg k_{r_1, r_2}, k_{s, r_1}, k_{s, r_2}$. An exact solution to this equation can be found, namely

$$\varphi_s = \omega_e t + 2 \arctan \left(-\frac{\Gamma}{\delta_{e0}} \right),$$

where $\Gamma = K_0 - \sqrt{\delta_{e0}^2 - K_0^2} \tan \left(\frac{1}{2} (t + c_1) \sqrt{\delta_{e0}^2 - K_0^2} \right)$, $\delta_{e0} = \omega_0 - \omega_e$, c_1 is an integration constant, and we assumed $\omega_e \neq \omega_0$. This equation shows a term with frequency ω_e plus another term that depends on t in a more complicated way. Let us assume, as we did in the main text, that K_0 is large enough, such that $K_0 > |\omega_0 - \omega_e|$. This implies that the term inside the square root in the above equation is negative. Let

$$K_1 = i\sqrt{K_0^2 - \delta_{e0}^2} = i\kappa,$$

and we have

$$\varphi_s = \omega_e t + 2 \arctan (F(t)),$$

where

$$F(t) = -\frac{K_0 - i\kappa \tan \left(\frac{1}{2} (t + c_1) i\kappa \right)}{\delta_{e0}}.$$

If we take the limit when t goes to infinity for the arctan term we have

$$\lim_{t \rightarrow \infty} \arctan (F(t)) = \arctan \left(\frac{K_0 + \kappa}{\omega_e - \omega_0} \right),$$

or

$$\arctan \left(\frac{K_0 + \sqrt{K_0^2 - (\omega_0 - \omega_e)^2}}{\omega_e - \omega_0} \right).$$

If $K_0 \gg |\omega_0 - \omega_e|$, then

$$\begin{aligned} \lim_{t \rightarrow \infty} \arctan (F(t)) &\approx \arctan \left(\frac{2K_0}{\omega_e - \omega_0} \right) \\ &\approx \pm \frac{\pi}{2}. \end{aligned}$$

So, for large K_0 and t ,

$$\varphi_s \approx \omega_e t \pm \pi$$

and

$$\varphi_{r_1} \approx \omega_e t \pm \pi.$$

We now turn to

$$\dot{\varphi}_{r_2} = \omega_0 + K_0 \sin (\varphi_{r_2} - \omega_e t - \pi).$$

The solution is

$$\varphi_{r_2} = \omega_e t - 2 \arctan \left(\frac{\Gamma'}{\delta_{e0}} \right),$$

where $\Gamma' = K_0 + \sqrt{\delta_{e0}^2 - K_0^2} \tan \left(\frac{1}{2} (t + c_2) \sqrt{\delta_{e0}^2 - K_0^2} \right)$, and c_2 is another integration constant. Following the same arguments as before, we obtain

$$\begin{aligned} \lim_{t \rightarrow \infty} \arctan (F(t)) &\approx \arctan (0) \\ &\approx 0, \end{aligned}$$

or, for large K_0 and t ,

$$\varphi_{r_2} \approx \omega_e t.$$

Of course, the above arguments only tell us the behavior of the equations when t goes to infinity, but in our models we deal with finite times. To better understand how fast the solution converges to $\omega_e t \pm \pi$ or $\omega_e t$, let us rewrite equation

$$\varphi_s = \omega_e t + 2 \arctan \left(-\frac{\Gamma}{\delta_{\epsilon 0}} \right)$$

in terms of dimensionless quantities. Let $\gamma = (\omega_e - \omega_0) / K_0$, then

$$\begin{aligned} \varphi_s = \omega_e t \\ + 2 \arctan \left(\frac{1}{\gamma} - \frac{\sqrt{\gamma^2 - 1}}{\gamma} \tan \left(\frac{(t + c_1) K_0 \sqrt{\gamma^2 - 1}}{2} \right) \right). \end{aligned}$$

Since γ is real and $\gamma \ll 1$ for large values of K_0 , we rewrite

$$\begin{aligned} \varphi_s = \omega_e t \\ + 2 \arctan \left(\frac{1 + \sqrt{1 - \gamma^2} \tanh \left(\frac{K_0(t + c_1) \sqrt{1 - \gamma^2}}{2} \right)}{\gamma} \right). \end{aligned}$$

We're only interested in the last term,

$$2 \arctan \left(\frac{1 + \sqrt{1 - \gamma^2} \tanh \left(\frac{K_0(t + c_1) \sqrt{1 - \gamma^2}}{2} \right)}{\gamma} \right). \quad (\text{Appendix A.92})$$

But for large values of t ,

$$\tanh \frac{K_0(t + c_1) \sqrt{1 - \gamma^2}}{2}, \quad (\text{Appendix A.93})$$

which is equal to

$$\frac{e^{\frac{K_0}{2}(t + c_1) \sqrt{1 - \gamma^2}} - e^{-\frac{K_0}{2}(t + c_1) \sqrt{1 - \gamma^2}}}{e^{\frac{K_0}{2}(t + c_1) \sqrt{1 - \gamma^2}} + e^{-\frac{K_0}{2}(t + c_1) \sqrt{1 - \gamma^2}}},$$

goes to 1. In fact, (Appendix A.93), and therefore (Appendix A.92), shows a characteristic time

$$t_c = \frac{2}{K_0 \sqrt{1 - \gamma^2}} = \frac{2}{\sqrt{K_0^2 - (\omega_e - \omega_0)^2}}.$$

Thus, for $t > t_c$ and for large K_0 (i.e., $K_0 \gg |\omega_e - \omega_0|$), a good approximation for φ_s is

$$\varphi_s \approx \omega_e t \pm \pi.$$

Similar arguments can be made for φ_{r_1} and φ_{r_2} .

Appendix A.6. Effectiveness of Reinforcement for the Oscillator Model

Here we show how to compute K' from the behavioral parameter θ and the other oscillator parameters. First, K_0 satisfies the normal distribution density

$$p(K_0) = \frac{1}{\sigma\sqrt{2\pi}} e^{-\frac{1}{2\sigma^2}(K_0 - \bar{K}_0)^2}, \quad (\text{Appendix A.94})$$

where σ is the standard deviation. The sigmoid function

$$\epsilon(K_0) = \frac{\epsilon_0}{1 + e^{-\gamma(K_0 - K')}} \quad (\text{Appendix A.95})$$

determines whether the couplings are affected. We also assume that the time of reinforcement, Δt_e , is large compared to $1/\epsilon$, as discussed in the text. If $\gamma \gg 1$, $\epsilon(K_0)$ approaches a Heaviside function $H(K_0)$ as $\epsilon(K_0) \approx \epsilon_0 H(K_0 - K')$. Thus, for large values of γ , learning happens only if $K_0 > K'$, and the probability of an oscillator reinforcement being effective

$$\theta = \frac{1}{\sigma\sqrt{2\pi}} \int_{K'}^{\infty} e^{-\frac{1}{2\sigma^2}(K_0 - \bar{K}_0)^2} dK_0, \quad (\text{Appendix A.96})$$

or

$$\theta = \frac{1}{2} \left(1 + \operatorname{erf} \left(\frac{\sqrt{2} \bar{K}_0 - K'}{2\sigma} \right) \right). \quad (\text{Appendix A.97})$$

Since θ is monotonically decreasing with K' , it is possible to solve the above equation for K' . For example, if we set $\theta' = .19$ we obtain that

$$\bar{K}_0 - K' = -0.8779\sigma. \quad (\text{Appendix A.98})$$

Choosing $\sigma = 10$ and $\bar{K}_0 = 100$, from (Appendix A.98) we obtain $K' = 187.79$.

References

- Acebron, J. A., Bonilla, L. L., Vicente, C. J. P., Ritort, F., Spigler, R., 2005. The kuramoto model: A simple paradigm for synchronization phenomena. *Reviews of Modern Physics* 77 (1), 137–185.
- Billock, V. A., Tsou, B. H., 2005. Sensory recoding via neural synchronization: integrating hue and luminance into chromatic brightness and saturation. *J. Opt. Soc. Am. A* 22 (10), 2289–2298.
- Billock, V. A., Tsou, B. H., 2011. To honor fechner and obey stevens: Relationships between psychophysical and neural nonlinearities. *Psychological Bulletin* 137 (1), 1–18.
- Bower, G., 1961. Application of a model to paired-associate learning. *Psychometrika* 26, 255–280.
- Bower, J. M., Beeman, D., 2003. *The Book of Genesis: Exploring Realistic Neural Models with the General NEural SIMulation System*. Internet Edition.
URL <http://www.genesis-sim.org/GENESIS>
- Bruza, P., Busemeyer, J., Gabora, L., 2009. Introduction to the special issue on quantum cognition. *Journal of Mathematical Psychology* 53, 303–305.
- Busemeyer, J. R., Wang, Z., Townsend, J. T., 2006. Quantum dynamics of human decision-making. *Journal of Mathematical Psychology* 50, 220–241.
- de Barros, J. A., Carvalhaes, C. G., de Mendonca, J. P. R. F., Suppes, P., 2006. Recognition of words from the eeg laplacian. *Revista Brasileira de Engenharia Biomedica* 21, 45–59.

- de Barros, J. A., Suppes, P., 2009. Quantum mechanics, interference, and the brain. *Journal of Mathematical Psychology* 53, 306–313.
- Dickinson, A., 1980. *Contemporary animal learning theory*. Cambridge Univ Press, Cambridge, Great Britain.
- Eckhorn, R., Bauer, R., Jordan, W., Brosch, M., Kruse, W., Munk, M., Reitboeck, H., 1988. Coherent oscillations: A mechanism of feature linking in the visual cortex? *Biological Cybernetics* 60 (2), 121–130.
- Eeckman, F. H., Freeman, W. J., 1991. Asymmetric sigmoid non-linearity in the rat olfactory system. *Brain Research* 557, 13–21.
- Estes, W. K., 1950. Toward a statistical theory of learning. *Psychological Review* 57 (2), 94–107.
URL <http://psycnet.apa.org/journals/rev/57/2/94/>
- Estes, W. K., 1959. Component and pattern models with markovian interpretations. In: Bush, R. R., Estes, W. K. (Eds.), *Studies in Mathematical Learning Theory*. Stanford University Press, Stanford, CA, pp. 9–52.
- Freeman, W. J., 1979. Nonlinear dynamics of paleocortex manifested in the olfactory eeg. *Biological Cybernetics* 35, 21–37.
- Freeman, W. J., Barrie, J. M., 1994. *Temporal Coding in the Brain*. Springer, New York, Ch. Chaotic oscillations and the genesis of meaning in cerebral cortex, pp. 13–37, corrected Internet edition, available at <http://sulcus.berkeley.edu/wjf/AB.Genesis.of.Meaning.pdf>.
- Friedrich, R. W., Habermann, C. J., Laurent, G., 2004. Multiplexing using synchrony in the zebrafish olfactory bulb. *Nature neuroscience* 7 (8), 862–871.
- Gerstner, W., Kistler, W., 2002. *Spiking Neuron Models*. Cambridge University Press, Cambridge.
- Guckenheimer, J., Holmes, P., 1983. *Nonlinear Oscillations, Dynamical Systems, and Bifurcation of Vector Fields*. Springer-Verlag, New York.
- Hoppensteadt, F. C., Izhikevich, E. M., 1996a. Synaptic organizations and dynamical properties of weakly connected neural oscillators i. analysis of a canonical model. *Biological Cybernetics* 75 (2), 117–127.
- Hoppensteadt, F. C., Izhikevich, E. M., 1996b. Synaptic organizations and dynamical properties of weakly connected neural oscillators ii. learning phase information. *Biological Cybernetics* 75 (2), 129–135.
- Izhikevich, E. M., 2007. *Dynamical Systems in Neuroscience: The Geometry of Excitability and Bursting*. The MIT Press, Cambridge, Massachusetts.
- Kazantsev, V. B., Nekorkin, V. I., Makarenko, V. I., Llinas, R., 2004. Self-referential phase reset based on inferior olive oscillator dynamics. *Proceedings of the National Academy of Sciences of the United States of America* 101 (52), 18183–18188.
- Keeping, E. S., 1995. *Introduction to statistical inference*. Dover Publications Inc., Mineola, New York.
- Kuramoto, Y., 1984. *Chemical Oscillations, Waves, and Turbulence*. Dover Publications, Inc., Mineola, New York.
- Leznik, E., Makarenko, V., Llinas, R., 2002. Electrotonically Mediated Oscillatory Patterns in Neuronal Ensembles: An In Vitro Voltage-Dependent Dye-Imaging Study in the Inferior Olive. *J. Neurosci.* 22 (7), 2804–2815.

- Luce, R. D., 1986. *Response Times*. Oxford University Press, New York.
- Lutz, A., Lachaux, J.-P., Martinerie, J., Varela, F. J., 2002. Guiding the study of brain dynamics by using first-person data: Synchrony patterns correlate with ongoing conscious states during a simple visual task. *Proceedings of the National Academy of Sciences* 99 (3), 1586–1591.
- Lytton, W. W., Sejnowski, T. J., 1991. Simulations of cortical pyramidal neurons synchronized by inhibitory interneurons. *J Neurophysiol* 66 (3), 1059–1079.
- Murthy, V. N., Fetz, E. E., 1992. Coherent 25- to 35-Hz Oscillations in the Sensorimotor Cortex of Awake Behaving Monkeys. *Proceedings of the National Academy of Sciences* 89 (12), 5670–5674.
- Nishii, J., 1998. A learning model for oscillatory networks. *Neural Networks* 11 (2), 249–257.
- Nunez, P., Srinivasan, R., 2006. *Electric Fields of the Brain: The Neurophysics of EEG*, 2nd Ed. Oxford University Press.
- Park, E.-H., Soa, P., Barreto, E., Gluckman, B. J., Schi, S. J., 2003. Electric field modulation of synchronization in neuronal networks. *Neurocomputing* 52-54, 169–175.
- Rees, G., Kreiman, G., Koch, C., 2002. Neural correlates of consciousness in humans. *Nat Rev Neurosci* 3 (4), 261–270.
- Rodriguez, E., George, N., Lachaux, J.-P., Martinerie, B. R., Varela, F. J., 1999. Perception’s shadow: long-distance synchronization of human brain activity. *Nature* 397, 430–433.
- Seliger, P., Young, S. C., Tsimring, L. S., 2002. Plasticity and learning in a network of coupled phase oscillators. *Physical Review E* 65, 041906–1–7.
- Sompolinsky, H., Golomb, D., Kleinfeld, D., 1990. Global Processing of Visual Stimuli in a Neural Network of Coupled Oscillators. *PNAS* 87 (18), 7200–7204.
- Steinmetz, P. N., Roy, A., Fitzgerald, P. J., Hsiao, S. S., Johnson, K. O., Niebur, E., 2000. Attention modulates synchronized neuronal firing in primate somatosensory cortex. *Nature* 404 (6774), 187–190.
- Strogatz, S. H., 2000. From kuramoto to crawford: exploring the onset of synchronization in populations of coupled oscillators. *Physica D: Nonlinear Phenomena* 143 (1-4), 1–20.
- Suppes, P., 1959. A linear learning model for a continuum of responses. In: Bush, R. R., Estes, W. K. (Eds.), *Studies in Mathematical Learning Theory*. Stanford University Press, Stanford, CA, pp. 400–414.
- Suppes, P., 1960. Stimulus-sampling theory for a continuum of responses. In: K. Arrow, S. K., Suppes, P. (Eds.), *Mathematical Methods in the Social Sciences, 1959; proceedings of the first Stanford Symposium*. Stanford University Press, Stanford, CA, Ch. 23, pp. 348–365.
- Suppes, P., Oct. 1969. Stimulus-response theory of finite automata. *Journal of Mathematical Psychology* 6 (3), 327–355.
 URL <http://www.sciencedirect.com/science/article/pii/S0022249669900108>
- Suppes, P., 2002. *Representation and Invariance of Scientific Structures*. CSLI Publications, Stanford, CA.
- Suppes, P., Atkinson, R. C., 1960. *Markov Learning Models for Multiperson Interactions*. Stanford University Press, Stanford, CA.

- Suppes, P., de Barros, J. A., 2007. Quantum mechanics and the brain. In: *Quantum Interaction: Papers from the AAAI Spring Symposium*. Technical Report SS-07-08. AAAI Press, Menlo Park, CA, pp. 75–82.
- Suppes, P., Frankmann, R., 1961. Test of stimulus sampling theory for a continuum of responses with unimodal noncontingent determinate reinforcement. *Journal of Experimental Psychology* 61 (2), 122–132.
- Suppes, P., Ginsberg, R., 1963. A fundamental property of all-or-none models, binomial distribution of responses prior to conditioning, with application to concept formation in children. *Psychological Review* 70, 139–161.
- Suppes, P., Han, B., 2000. Brain-wave representation of words by superposition of a few sine waves. *Proceedings of the National Academy of Sciences* 97, 8738–8743.
- Suppes, P., Han, B., Epelboim, J., Lu, Z.-L., 1999a. Invariance between subjects of brain wave representations of language. *Proceedings of the National Academy of Sciences* 96, 12953–12958.
- Suppes, P., Han, B., Epelboim, J., Lu, Z.-L., 1999b. Invariance of brain-wave representations of simple visual images and their names. *Proceedings of the National Academy of Sciences* 96, 14658–14663.
- Suppes, P., Han, B., Lu, Z.-L., 1998. Brain-wave recognition of sentences. *Proceedings of the National Academy of Sciences* 95, 15861–15866.
- Suppes, P., Lu, Z.-L., Han, B., 1997. Brain wave recognition of word. *Proceedings of the National Academy of Sciences* 94, 14965–14969.
- Suppes, P., Perreau-Guimaraes, M., Wong, D., 2009. Partial orders of similarity differences invariant between eeg-recorded brain and perception representations of language. *Neural Computation* 21, 3228–3269.
- Suppes, P., Rouanet, H., Levine, M., Frankmann, R. W., 1964. Empirical comparison of models for a continuum of responses with noncontingent bimodal reinforcement. In: Atkinson, R. C. (Ed.), *Studies in Mathematical Psychology*. Stanford University Press, Stanford, CA, pp. 358–379.
- Tallon-Baudry, C., Bertrand, O., Fischer, C., 2001. Oscillatory Synchrony between Human Extrastriate Areas during Visual Short-Term Memory Maintenance. *J. Neurosci.* 21 (20), 177RC–1–5.
- Trevisan, M. A., Bouzat, S., Samengo, I., Mindlin, G. B., 2005. Dynamics of learning in coupled oscillators tutored with delayed reinforcements. *Physical Review E (Statistical, Nonlinear, and Soft Matter Physics)* 72 (1), 011907–1–7.
- Vassilieva, E., Pinto, G., de Barros, J., Suppes, P., 2011. Learning pattern recognition through quasi-synchronization of phase oscillators. *IEEE Transactions on Neural Networks* 22 (99), 84–95.
- Wang, D., 1995. Emergent synchrony in locally coupled neural oscillators. *Neural Networks, IEEE Transactions on Neural Networks* 6 (4), 941–948.
- Winfree, A. T., 2002. OSCILLATING SYSTEMS: On Emerging Coherence. *Science* 298 (5602), 2336–2337.
- Wong, D. K., Uy, E. T., Guimaraes, M. P., Yang, W., Suppes, P., 2006. Interpretation of perceptron weights as construct time series for eeg classification. *Neurocomputing*In press.
- Wright, J., Liley, D., 1995. Simulation of electrocortical waves. *Biological Cybernetics* 72 (4), 347–356.
- Yamanishi, J.-i., Kawato, M., Suzuki, R., 1980. Two coupled oscillators as a model for the coordinated finger tapping by both hands. *Biological Cybernetics* 37 (4), 219–225.